Development of An Automated System for the Measurement of Focal Ratio Degradation of High Numerical Aperture Fibres

by

Jooyoung Lee
B.Sc., Dongguk University, 2015

A Thesis Submitted in Partial Fulfillment
of the Requirements for the Degree of

MASTER OF APPLIED SCIENCE

in the Department of Mechanical Engineering

Supervisory Committee

[Development of An Automated System for the Measurement of Focal Ratio Degradation of High Numerical Aperture Fibres]

by

Jooyoung Lee
B.Sc., Dongguk University, 2015

Supervisory Committee

Dr. Colin Bradley – Department of Mechanical Engineering
Co-Supervisor

Dr. Martin Byung-Guk Jun – Department of Mechanical Engineering
Co-Supervisor

Abstract

The thesis presents the development and testing of an automated fibre optic test system for the measurement of focal ratio degradation (FRD) in high numerical aperture fibres. In particular, the fibres under examination are being proposed for use in the Maunakea Spectroscopic Explorer (MSE), a new telescope currently being designed for wide-field surveys of the night sky. A critical subsystem of the MSE is the Fiber Transmission System (FiTS) that connects the focal plane to the telescope's spectrographs. In preparation for MSE-FiTS, a method of characterizing the focal ratio degradation (FRD), between the input and output of every fibre, of candidate multi-mode fibres is highly important. The ultimate goal is the testing of all 4,332 fibres after assembly and prior to installation on MSE. An optical bench has been constructed to test the performance of an automated characterization system; a variation on the collimated beam test. Herein we present the underlying analysis FRD measurement method, the optical design of the test bench, the motion control system and the software for measuring FRD, and controlling the automated test system. The open-source automation software is also introduced; the Big FiTS Fibre Wrapper (Big FFW). The results of tests performed using the Big FFW on samples of candidate fibres are presented and compared with the results in the literature using manual methods. The results suggest that the candidate MSE fibre meets the science requirement of less than 5% focal ratio degradation for an f/2 input beam measured at the fibre output. There is less than 1% disagreement between the automated measurement method and manual methods reported in the literature. The fully automated system can measure the FRD of up to 10 fibres in a typical MSE fibre bundle configuration.

Table of Contents

List of Tables

List of Figures

Acknowledgments

I would like to express my deep and sincere gratitude to:

My supervisor, Dr. Colin Bradley, for giving me a great opportunity to do research and providing invaluable guidance throughout this research. He has taught me a methodology to conduct research and present my research as clearly as possible. It was a great privilege and honor to work and study under his supervision.

Dr. Kim Venn, David Crampton, and Darren Erickson for giving me the opportunity to participate in an amazing project. I sincerely appreciate their professional support, advice and passionate participation through this project.

Dr. Martin Byung-guk Jun for giving me a great opportunity to study and complete M.ASc program at University of Victoria.

Farbod Jahandar, Stephanie Monty and Tarun Kumar for being wonderful friends and colleagues. I appreciate all the help and advice.

I also thank my friends, Sooyong Kim, Kaveh Nazeri, Arman Nikkhah, Mehran Farhadmanesh and Tim Seungwon Jun, for their help and assistance. Finally, I am extremely grateful to my parents and brother for providing me with unfailing support and constant encouragement. This accomplishment would not have been possible without them.

Dedication

To my parents, Kyung Soo Lee and Yong Rhan Chung.

Chapter 1 - The Maunkea Spectroscopic Explorer

The Maunakea Spectroscopic Explorer (MSE) will be an upgrade of the current 3.6m Canada-France-Hawaii Telescope (CFHT) into a 11.25m aperture, 1.5 square degree field of view telescope, fully dedicated to performing multi-object spectroscopy [1]-[4]. The MSE will provide low, medium and high-resolution spectroscopy across the full wavelength range of 0.36 − 1.8μm (UV to near-infrared). In contrast with most existing ground-based optical telescopes, the MSE will have massive multiplexing capability and will collect 4,332 spectra per exposure and an on-target observing efficiency of more than 80%.

Figure 1.1: Exterior views of CFHT (ventilation modules open) and MSE (ventilation modules closed). Courtesy of Kei Szeto MSE Project Office.

The telescope has a number of unique features:

- As shown in Figure 1.1, the foundation of the existing CFHT will be reused and the existing dome replaced by a Callotte style enclosed designed by Dynamic Structures Ltd (Port Coquitlam, B.C.).
- The new dome allows the existing telescope support structure and primary mirror (3.6 m) to be replaced with a more space efficient telescope structure (see Figure 1.2) and 11.25 m segmented primary mirror.
- Figure 1.2 also shows the primary mirror (M1 system) which is comprised of 60 individual 1.44 m hexagonal elements. The segmented mirrors are individually adjustable (tip-tilt control) to compensate for small changes in the overall mirror shape induced by gravitational sag.
- The two low and medium resolution spectrographs are housed on the Naysmith platform and in the observatory basement respectively.
- A Fiber Transmission System (FiTS) that is composed of 3,249 fibres that feed the low and medium resolution spectroscopes and 1083 fibres feeding the high-resolution spectrograph. As shown in Figure 1.2, the 4,332 fibres are encased in, and supported by, 57 fibre bundles; each bundle containing 76 fibres. The bundles run approximately 75 m from the prime focus location to the spectroscopes.
- At the focal plane, each fibre is interfaced with a “fibre positioner system” that can accurately move the tip of the fibre anywhere within its A x B patrol area. Each fibre positioner is controlled in 2-axes to follow a target across the sky as dictated by its individual path program. The path programs are created before each night’s viewing and account for factors such as exposure duration, target path, environmental conditions and neighboring positioner location.
- Each fibre delivers light from the focal plane to the appropriate spectroscope where the signal is analyzed for chemical composition.

The MSE will unveil the composition and dynamics of the faint Universe and is designed to excel at precision studies of faint astrophysical phenomena. This will enable unique and transformative science such as: the emergence of the Periodic Table of the elements; astrophysical exploration of the nature of dark matter; charting the growth of supermassive black holes; and, discovering the connection of galaxies to the large-scale structure of the Universe. The MSE is a wide-field imaging survey instrument and provides targets for the pointed follow-up by extremely large optical telescopes such as the Thirty Meter Telescope, the Giant Magellan Telescope, and the (European) Extremely Large Telescope, by providing the essential filtering of the immensely large survey datasets.

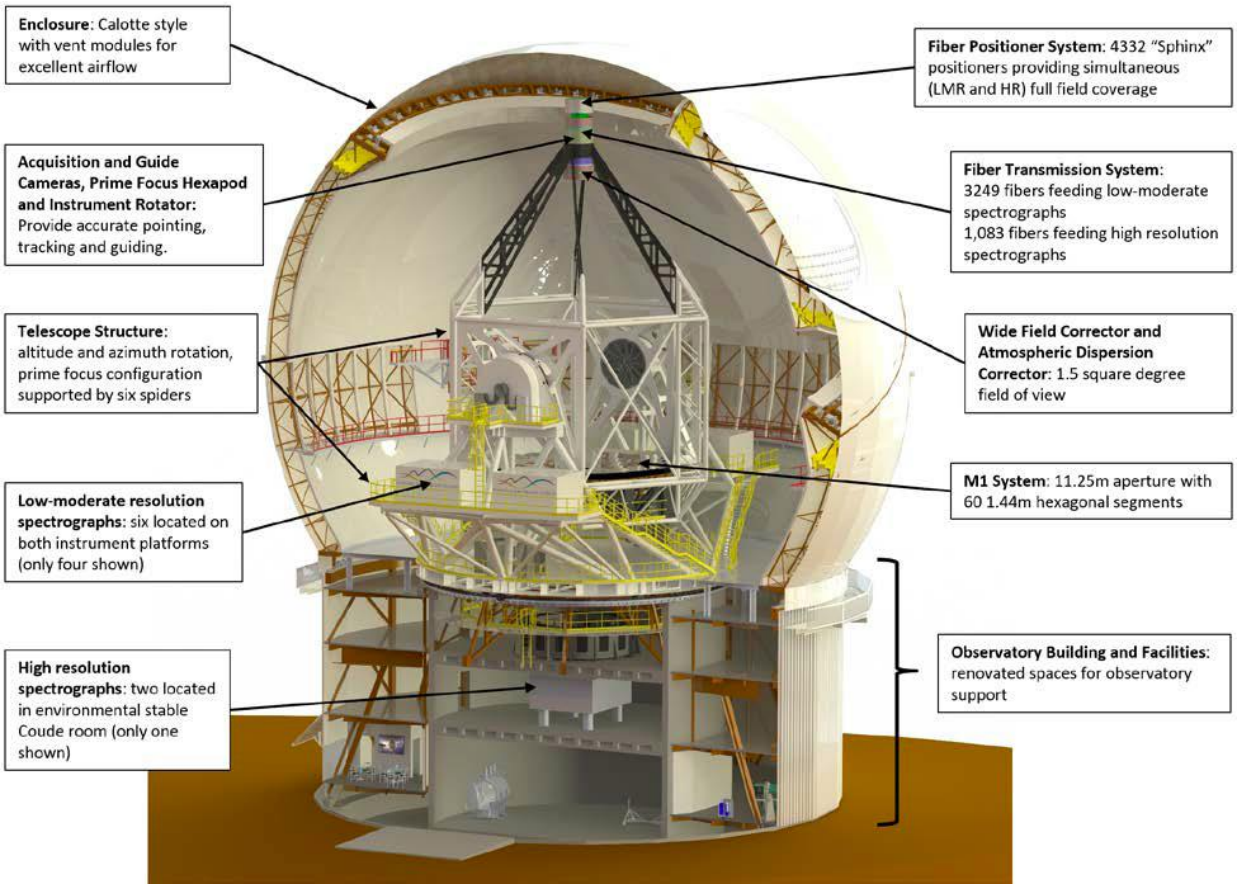

Figure 1.2: MSE observatory architecture detail showing all major sub-system elements.

The MSE Fibre Transmission System

A critical element of the MSE, and the focus of this thesis, is the Fiber Transmission System (FiTS). The FiTS will make use of more than 4,332 multi-mode optical fibres to deliver the light signals with the goal of near identical light delivery amongst all the fibres to within 1%. Through a specially designed fibre positioning system and fibre bundling assembly, FiTS will transmit the light from the prime focus ~ 35 m to the low-resolution spectrographs located in the telescope pier and ~ 50 m to the high-resolution spectrographs located on the Nasmyth platforms. In Figure 1.3, the FiTS fibre bundle routing is shown in blue (low and medium resolution spectrograph feeds) and red (high-resolution spectrograph feed). (see paper number 10702-284 of the same proceedings for more details [1]).

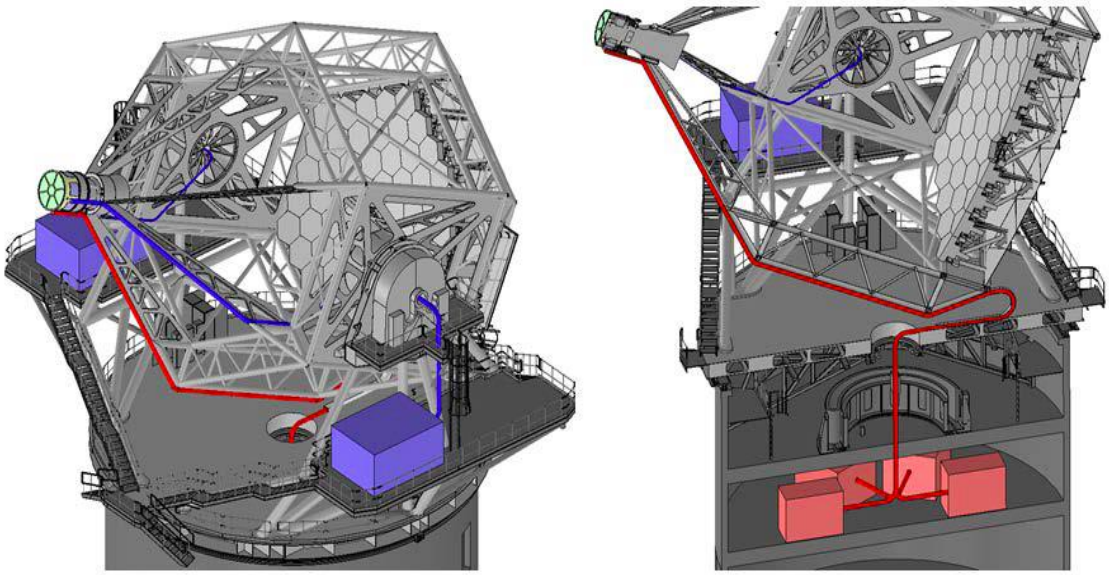

Figure 1.3: FiTS cable routing—LMR fibres (blue lines) and HR fibres (red lines). The colored boxes illustrate the conceptual locations of the spectrographs.

A critically important function of FiTS is providing the fibre bundle routing and handling for the fibres, through the observatory and over the full range of the telescope motion in two axes, and rotation. The fibre bundle path, from prime focus to spectrographs, is shown in Figure 1.4.

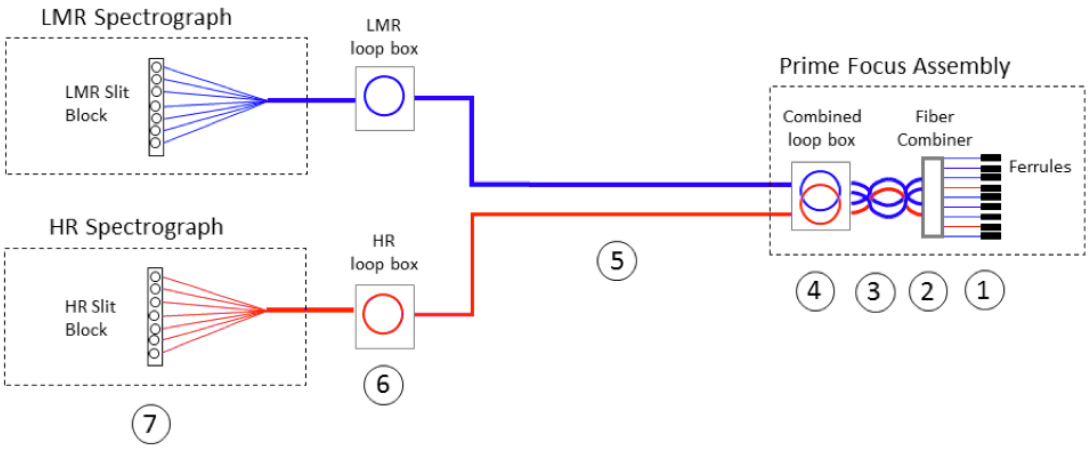

Figure 1.4: Cable schematic: the photons enter the fibres in the Prime Focus Assembly from the right. See below for descriptions of components 1–7.

We can trace the fibre cable by following light through the system (Figure 1.4):

1 Individual fibres are grouped into four protection tubes at the fibre combiner.

2 Three tubes contain 19 LMR fibres each, while a fourth tube contains 19 HR fibres. The four tubes exit the back of each fibre combiner.

3 The protection tubes are wound through a helical section, to provide rotation compliance with the end containing the positioners, ferrules, and fibre combiners, as rotated by InRo. Fibre tubes enter the first set of loop boxes at the fixed end of the helical section

4 Loop boxes provide access to bare fibres for splicing, in case repairs are needed.

5 Fibre cables are routed across the telescope structure (there are 57 fibres with spares in each LMR cable tube; 19 fibres plus spares in each HR cable tube).

6 A second set of loop boxes is located near the spectrographs, providing access to bare fibres should repair be necessary.

At the output, individual fibres are arranged into an array, using slit blocks. The slit blocks act as the entrance slits to the spectrographs (Figure 1.5). At the inputs of the spectrographs, the fibres terminate in slit blocks, which provide the interface between FiTS and the spectrographs. The mechanical interface to the spectrographs accommodates the fibre output slit geometry determined by the LMR and HR spectrograph designs. For

example, the shape of the slit compensates for optical distortion, such that spectra are projected onto the spectrograph detectors in straight columns (to maximize detector utilization).

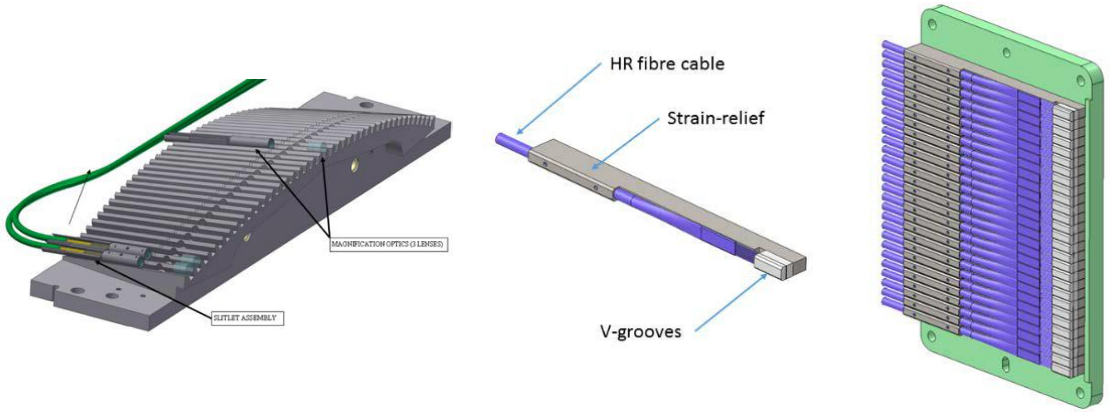

Figure 1.5: Left: Curved slit block. Right: V-grooves and strain-relief concepts for a straight slit input unit.

An important aspect of the FiTS design is to minimize fibre stress during observations. This will serve to reduce differential focal ratio degradation and far-field effects as the telescope moves across the sky, as well as to maintain uniform and stable throughput among the thousands of fibres. The characterization of focal ratio degradation (FRD) and its measurement on fibre bundles is the focus of this thesis and FRD is explained more fully in the next chapter.

One end of the FiTS is located at the primary focal plane, or "top end", of the telescope as shown in Figure 1.2. Here is located an array of fibre positioners and each fibre is fixed in its positioners using a "spine" (Figure 1.6). The spines carry the FiTS fibres and piezo actuators move them into position to collect light from science targets. Each spine assembly (Figure 1.6, top left- and right-hand panels) includes several components. A telescopic arrangement of two carbon fibre tubes forms each spine; each spine houses a FiTS fibre, together with its ferrule, and is supported by a pivot ball, held in place by a magnetic "cup," which acts as the fulcrum for the tilt motion. Driven by its control system, the piezo actuator contracts and expands. This produces a stick–slip motion at the cup and ball interface,

which translates into an angular displacement of the spine in tilt. The tilt of the carbon fibre tube produces lateral motion at the fibre end, moving it toward the target position on the focal surface.

FiTS is designed to maintain the highest possible throughput for the overall MSE system, so that the fibres are provided as a continuous link, without any connectors. High numerical aperture fibres (NA = 0.26–0.28) have been selected, capable of accepting the f/1.926 beam delivered by the telescope optics, in order to obviate the need for additional optics at the fibre input and avoid incurring the associated throughput losses. Throughput is affected by the fibres' length and transmission characteristics, particularly at the blue end of the wavelength spectrum.

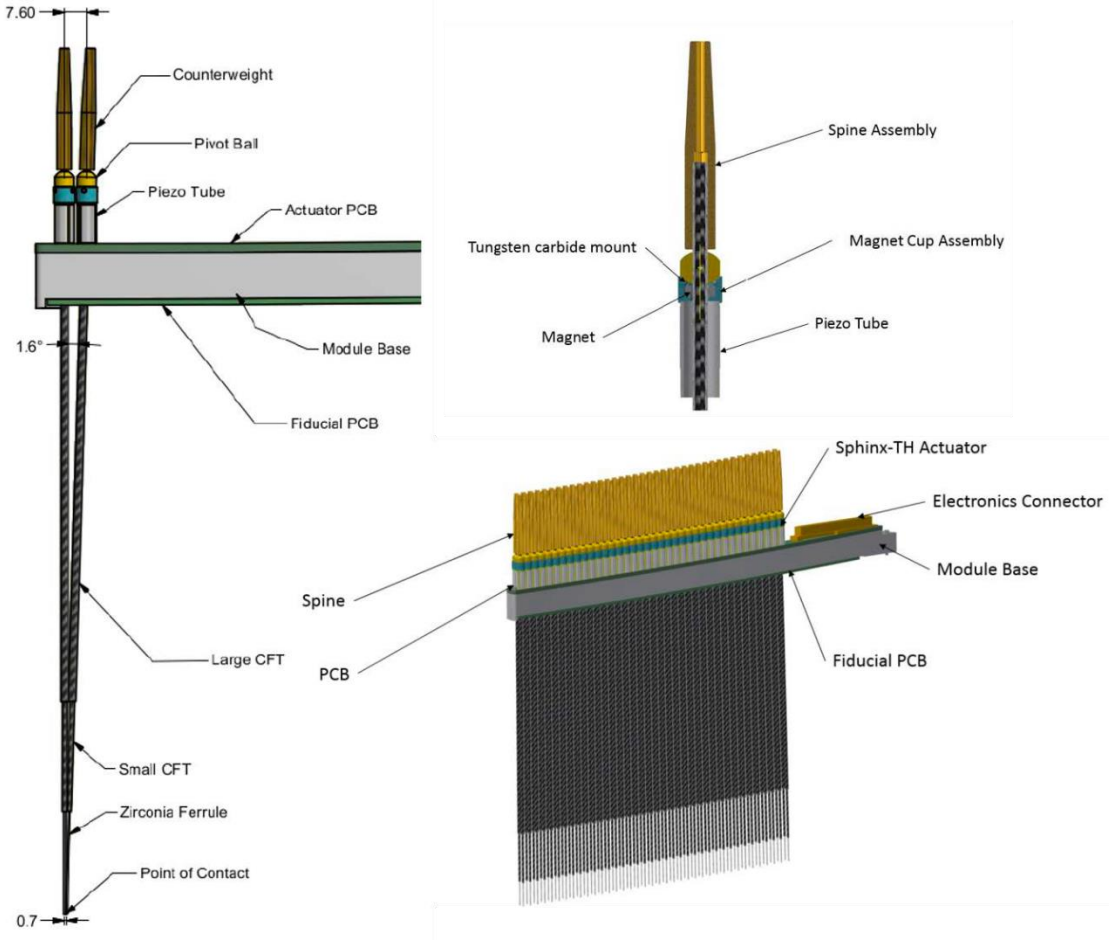

Figure 1.6: Sphinx fibre positioner module—Each module carries 76 spines, with 57 LMR and 19 HR fibres (bottom right), two adjacent spine assemblies (left) and a close-up of the piezo actuator (top right).

The current configuration (shown in Figure 1.2) houses the high-resolution spectrographs in the inner pier (50 m in length) and the low to medium resolution spectrographs on the instrument platforms (35 m in length). The spectral resolution, the degree of multiplexing (i.e., the total number of spectra), and wavelength range needed in each of the LR, MR, and HR configurations are prescribed by high-level science requirements. Observations using the HR spectrographs involve 1,083 fibres of 0.8 arcseconds (85 microns) in diameter, which feed two spectrographs, located in the Inner Pier spectrograph room. Observations using the LMR spectrographs involve 3, 249 fibres of 1.0 arcsecond (107 microns) in diameter, which feed a suite of six spectrographs, located on two spectrograph platforms, near the elevation axis of the telescope. The light enters the fibres at f/1.926, as delivered by the telescope, and exits at a faster focal ratio, due to the effects of focal ratio degradation. FRD from the fibres is assumed to be 5%. Both arrays of fibres (HR and LMR) are independently capable of full-field coverage at the focal surface, enabled by the large patrol area of the Sphinx positioners, which use tilting spine technology. During the integration of the fibres with the positioners, the HR and LMR fibres are distributed in the field of view (Figure 1.6), with their tips arranged on the convex focal surface.

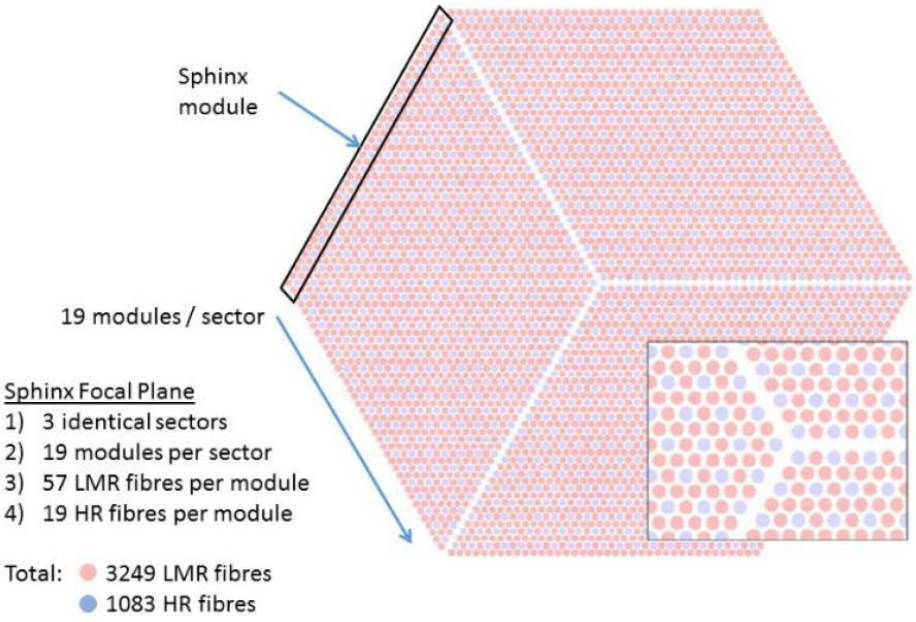

Figure 1.7: Sphinx positioner arrangement in the MSE focal plane. This fibre distribution gives full field coverage of both low-medium resolution fibres (pink) and high-resolution fibres (blue).

As the performance of FiTS is subject to both fibre characteristics and telescope dynamics, both need to be well understood prior to the construction of MSE. This requires the successful verification of fibre performance through measurements of individual fibres and fibre bundles, such as; fibre focal ratio degradation (FRD), throughput, general wavelength dependency, fibre cross-talk and any effects associated with fibre capping/splicing procedures. Additionally, the simulated effects of on-sky telescope dynamics on fibres must be tested. As part of the MSE FiTS project, we have constructed an automated fibre optic test bench to perform in-direct FRD measurements of MSE candidate fibres in a fast, efficient and consistent manner. This as an important facility not just in the context of MSE but also in the broader context of future fibre-fed instruments and multi-fibre positioning systems like TMT's WFOS [5] and E-ELT's MOSAIC [6] instruments and GMT's MANIFEST [7] fibre positioner. Here we present the details of the optical bench including; the optical components involved, automation hardware, and the software created to facilitate both measurements and analysis of the fibre FRD.

1.1 Thesis Objective

The goal of this thesis is to develop an automated, reliable and accurate method of measuring the FRD on all the fibres in a bundle. The automated testing of FRD will be critically important during manufacture of the fibre bundles to ensure that there is no fibre failing to meet the stringent performance requirements.

Chapter 2 - Focal Ratio Degradation Measurement in a Multi-Mode Optical Fibre

An optical fibre consists of two major components: core and cladding. Light injected into the fibre core, remains contained within the fibre core, and is transmitted along the length of the fibre due to the process of total internal reflection of the light signal at the interface between the core and the cladding. The refractive index of the cladding is greater than the refractive index of the core. Optical fibres are classified as single-mode or multi-mode; a single mode fibre only transmits the fundamental mode of the light signal, whereas a multimode fibre allows transmission of the fundamental and higher order modes. The type of fibre classification is dictated by the diameter of the core; a single mode fibre's core diameter is smaller (typically on the order of 5 to 20 microns) than a multi-mode fibre (typically 100 to 250 microns).

The diagram of Figure 2.1 below shows the cross-sectional structure of a single mode fibre where the core diameter is 10 µm and the cladding is 125 µm. The outer layer is a protective jacket that does not carry any light signal. Single mode fibres are mainly used in optical communication systems where it is critical to maintain the fidelity of each optical pulse over a long distance. Single mode fibres are also used in fibre sensors that utilise the interference phenomenon to detect small light phase differences between a reference and sensing arm (e.g. Mach Zehnder style of the interferometer)

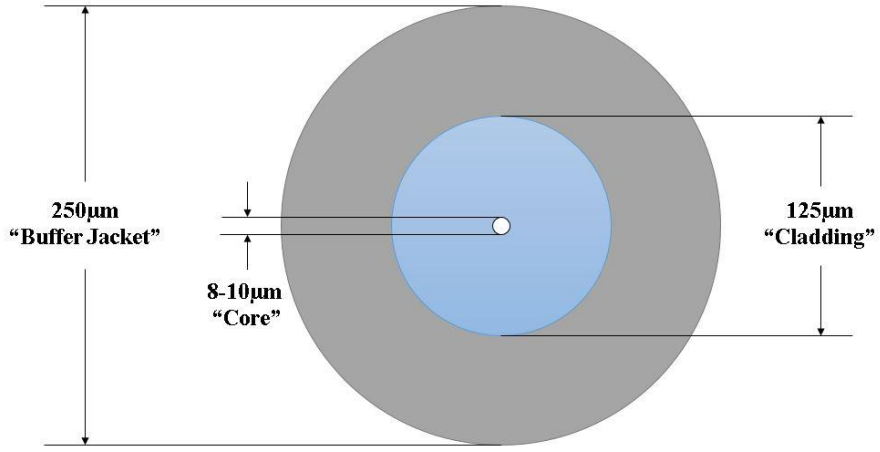

Figure 2.1: Cross section of a singlemode fibre

A multi-mode optical fibre has a comparatively large core surrounded by a cladding of a lower refractive index. Multimode fibres are designed to transmit spatially incoherent or multimode sources of light and can propagate hundreds of modes along its length.

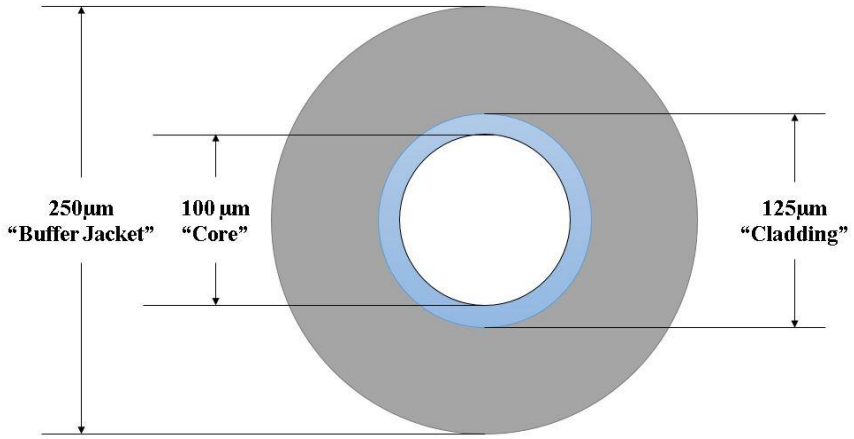

Figure 2.2: Cross section of a multimode fibre

2.1 Focal Ratio Degradation

Focal ratio degradation (FRD) is a result of irregularities, such as microbends [9] in the fibre, and heavily depends on fibre finishing procedures including cleaving and polishing of a surface of an optical fibre end [12]. Many research papers have investigated FRD and have shown that it is a wavelength dependent effect [8],[11],[12]. FRD has the physical effect of decreasing the input beam's focal ratio as measured at the fibre's output end. The physically manifests as an increased "spreading" of the output beam at the fibre output. This process can be described by the theoretical model of Gloge [13], which uses the power loss through a fibre, modelled as a cylindrical waveguide, to examine the power loss within the fibre due to scattering at the core-cladding interface. Gloge also shows that by imaging the far-field (FF) intensity pattern, one can recover the modal power distribution of the fibre within which the associated FRD loss is encoded. Further work by Gambling, Payne and Matsumura [14] and Carrasco and Parry [9], takes the model of Gloge and isolates a measurable quantity 'D' for the case of a well-characterized input beam, in particular, a collimated input beam. They also show that the far-field intensity pattern, resulting from a

collimated input beam, is a ring of light centred about the optical axis. The light ring has a finite radial thickness measurable as a Gaussian distribution in cross-section. Two important facts emerge from this analysis:

- The overall ring radius is related to the angle of the input beam.
- The ring's radial thickness is related to the micro-bending measurable D.

Figure 2.3 shows that FRD is proportional to the number of rays scattered radially compared to those scattered azimuthally, with pure azimuthal scattering being ideal [15]. Two examples of representative FF intensity patterns are shown in Figure 2.3. When fibres A and B have the same incident light angle, the diameters of both output rings are the same, but the thickness of the rings are relatively different. Fibre B has a thicker annulus than fibre A. It indicates that there is more light scattered to the central zone and periphery of the fibre B than fibre A. If more light is scattered, then the resulting loss of the light is greater. The example fibre A exhibits a better FRD than the example fibre B. Therefore, by constructing an optical test arrangement where a collimated beam is injected, at various angles, into the multimode fibre and for which the output FF intensity pattern is examined, the FRD can be measured indirectly in a simple and consistent manner.

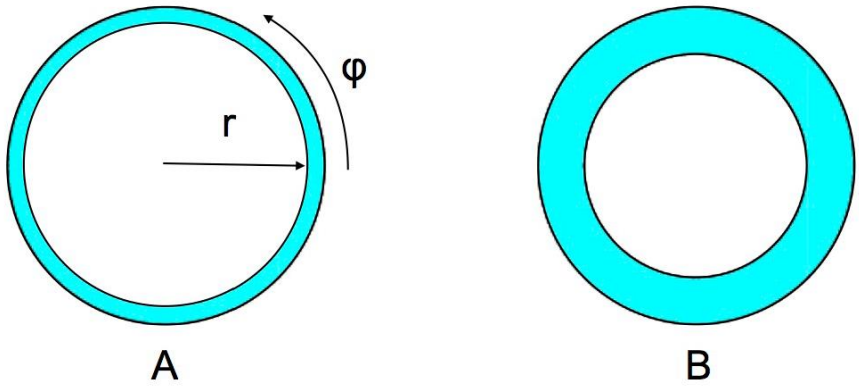

Figure 2.3: Representations of the ring test result from two different fibres, using identical injection angles. Fibre A has much better FRD than Fibre B, where most of the rays are scattered azimuthally instead of radially, as in the case of Fibre B.

2.2 Focal Ratio Degradation Measurement – the Ring Test

The FRD measurement using an input collimated beam in the "ring test" arrangement is shown below in Figure 2.4. In this work, the FRD of fibres with very similar properties to those planned for use in the MSE FiTS are used.

The input f-number is correlated with the incident angle of the input light. When the collimated beam is injected into the fibre core with a high incident angle, the output image doesn't exhibit a centrally concentrated light pattern but shows a ring-like pattern. Figure 2.4 shows the simplified schematic of the ring test.

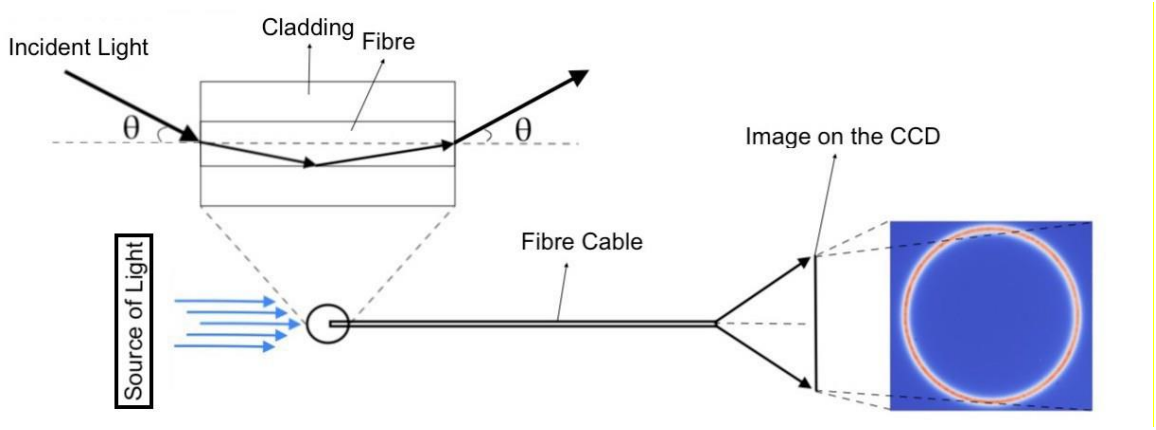

Figure 2.4: Simplified schematic of the ring test showing the injection of the collimated beam at a given input angle and the resulting far-field ring pattern.

	Incident Angle	Far-field images of output
0°	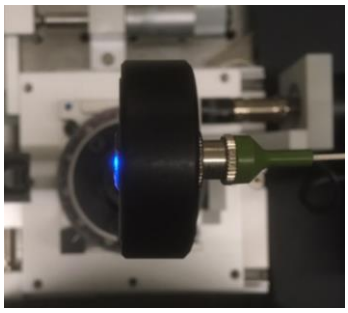	
7°	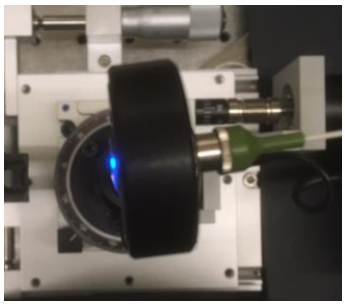	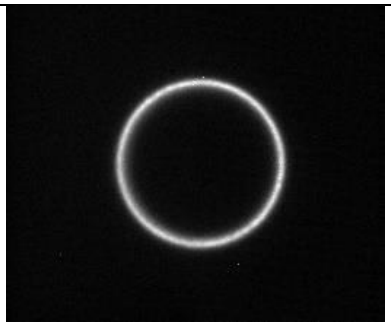
10°	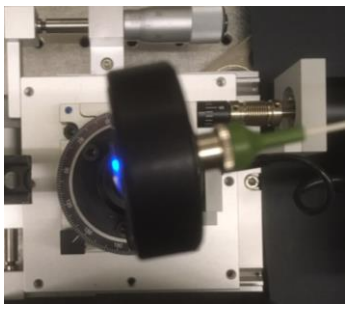	
14°	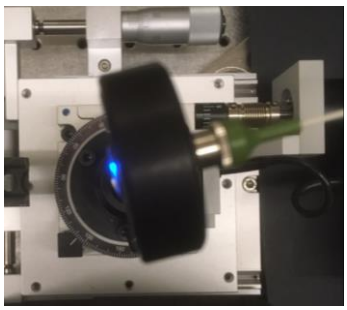	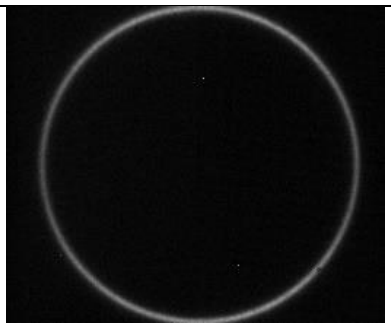

Figure 2.5: The collimated light injected into the optical fibre at different incident angles (Left), and its corresponding far-field ring-pattern images (Right).

As collimated light is injected into an optical fibre at increasing angles of incidence, the FF output images evolve from a concentrated central light disc to a ring-pattern (as shown in Figure 2.5). Two important metrics are collected from the FF ring image:

1. The diameter of the ring.
2. The annular thickness of the ring, as measured using the Full Width at Half Maximum (FWHM) technique.

FWHM is a common technique to define a width of the beam. FWHM can be defined as the distance between two points of 50% of the maximum peak value. The value of the measured FWHM is then converted to its corresponding $1/e^2$ value. $1/e^2$ is defined as the distance between two points where the optical intensity drops to about 13.5% of the peak value. In complicated intensity pattern graph, such as Gaussian beam profile, $1/e^2$ is generally used as a width of the beam, and the relationship between FWHM and $1/e^2$ can be defined by Equation 2.1.

$$2w = \frac{\sqrt{2}FWHM}{\sqrt{ln2}} \tag{2.1}$$

where $2w$ is full width of the beam at $1/e^2$

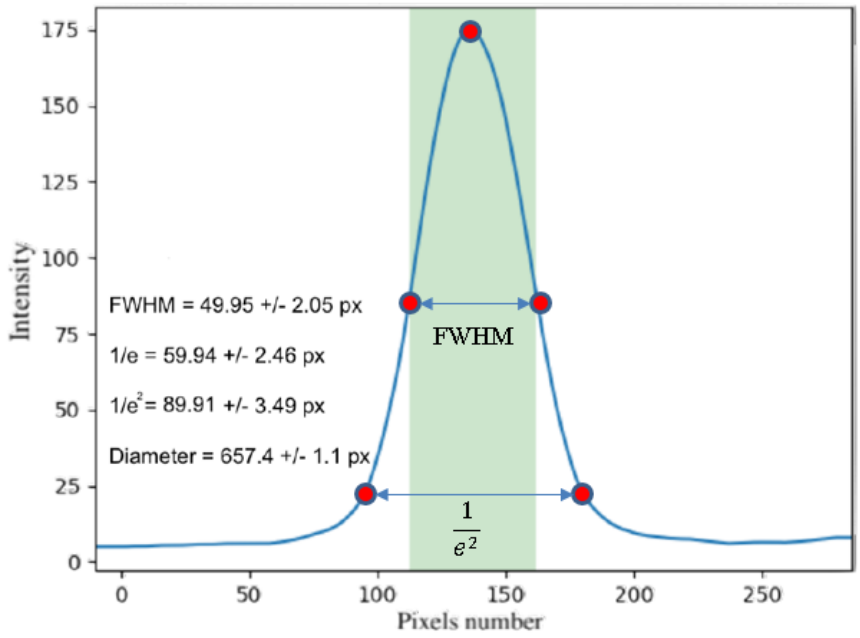

Figure 2.6: Full Width at Half Maximum (FWHM) points and $1/e^2$ of the Gaussian graph.

The ratio of this $1/e^2$ value to the diameter of the ring is then used to determine the relative FRD of the system. This method quantitatively determines the FRD of optical systems with different f ratios. The FRD proxy measurement is defined by Equation 2.2.

$$FRD = \frac{1/e^2}{Diameter} \tag{2.2}$$

Furthermore, the f-number can be determined based on the incident angle of the light through Equation 2.3.

$$F_{in} = \frac{1}{(2 \tan \theta_i)} \tag{2.3}$$

Where θ_i is the incident angle of the input light.

2.3 Numerical Aperture

The numerical aperture (NA) is a basic characteristic of optical fibre. NA represents the range of angles over which the fibre can accept the light. The light enters the optical fibre conically and half of the incident angle is called the acceptance angle. As shown in Figure 2.7 and Equation 2.4, the maximum angle at which a fibre can accommodate light is determined by the refractive index of the core and cladding of the optical fibre. The relationship between the acceptance angle of the input light and the numerical aperture can be defined by Equation 2.5 below.

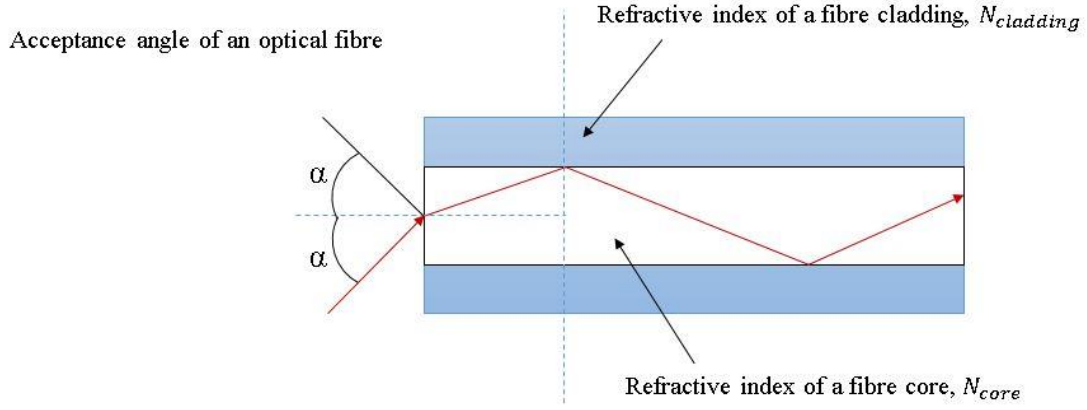

Figure 2.7: Numerical Aperture of a multimode fibre.

$$NA = sin\alpha = \sqrt{n^2_{Core} - n^2_{Cladding}} \quad (2.4)$$

$$Full\ Acceptance\ angle\ of\ the\ optical\ fibre = 2\alpha \quad (2.5)$$

Chapter 3 – Focal Ratio Degradation Measurement of a Single Multi-Mode Fibre

In order to experimentally evaluate FRD on "MSE-like fibres", the same fibre used in the Gemini Remote Access CFHT ESPaDOnS Spectrograph (GRACES) project [16] has been utilised. The GRACES project is an innovative instrumentation experiment that connects the ESPaDOnS (a bench-mounted high-resolution optical spectrograph at the Canada France Hawaii Project) using a 270-m long fibre from the nearby Gemini-North telescope. The losses are low enough to remain competitive with conventional spectrographs on other 8 to 10-m telescopes. This result is made possible by using FBP-type (FBP-type fibre is designed to operate over a very broad range of wavelength) of optical fibres made by Polymicro Technologies and by keeping the critical focal ratio degradation (FRD) losses to less than 10%.

For the ring test measurement of single multi-mode fibre, a GRACES fibre has been utilised with the following specification:

- A protective buffer of diameter 170 µm.
- A cladding diameter of 144 µm.
- A core diameter of 120 µm.
- The overall fibre length of 3m in length.
- Fibre numerical aperture is 0.26 ± 0.02, and this optical fibre can accommodate an input beam of f-number 2.

3.1 Experimental Setup for the Ring Test

The optical test bench was initially constructed to perform the ring test manually, testing fibres with known FRD characteristics to ensure repeatability of the test bench. Components of the setup were then identified for automation in addition to identifying a consistent post-processing method and analysis procedure. The final optical bench was designed using existing laboratory hardware and Python software. The software is compatible with any operating system and is written in an entirely modular form. The complete automated system, for the ring test, includes the automated hardware, the post-

processing and analysis software algorithms and the master software wrapper. The Python wrapper is used to wrap other existing scripts to call and extend the behavior of functions.

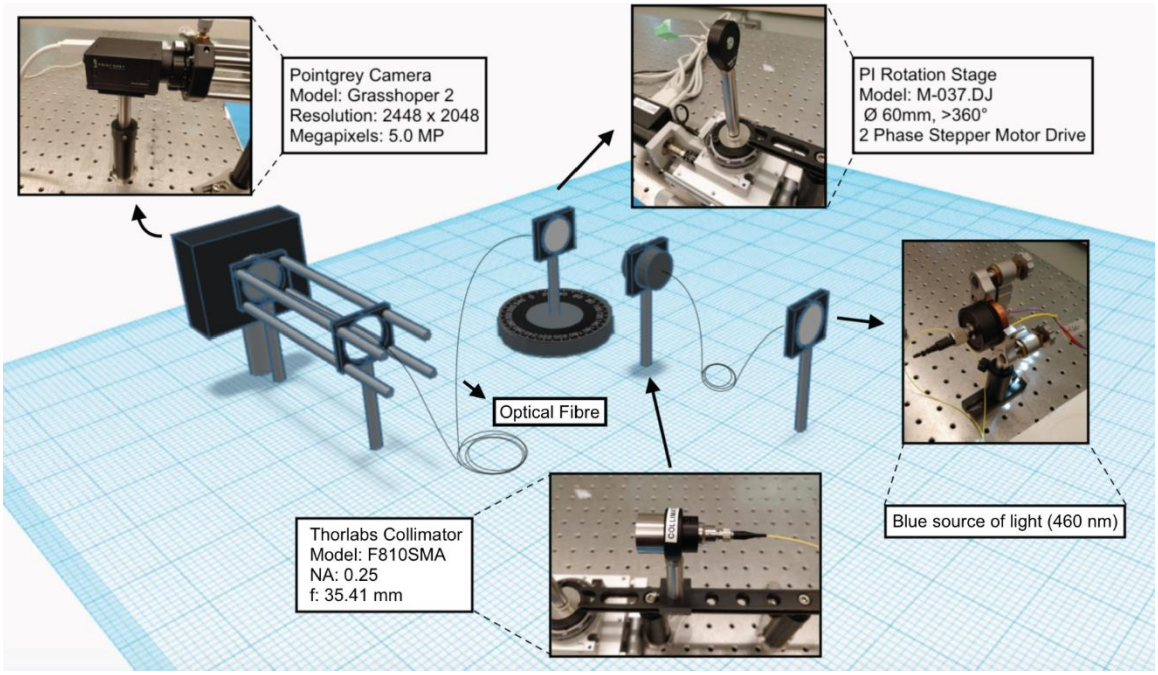

Figure 3.1: Full schematic of the ring test optical bench components.

Figure 3.1 shows the complete setup for the ring test which consists of a high-resolution 4,000 pixel resolution camera; a high precision rotational stage (nm scale); an optical beam collimator; two optical fibres and a blue light source with a wavelength of 460 nm.

The camera selected for the measurements was the Point Grey (GRAS-50S5M-C). This camera was selected due in part to the associated FlyCapture software and the Python wrapper, PyCapture2. FlyCapture is a software development kit (SDK) for image capture and camera control. It allows the user to select many camera attributes, such as the gain and exposure time (shutter speed). Furthermore, the software has a fully automatic mode that allows camera operation under the software control. PyCapture2 can be imported into any Python program and be used to connect the camera, capture the images, format the images and control camera characteristics. The rotation stage was automated using a Mercury Controller, made by Physik Instrumente, and accompanying Python wrapper PiPython. Using PiPython, the stage was connected, the current rotational position tracked

and the movements were specified in degree increments. Individual modules were created to control both the camera and the stage, with input and output shown in Figure 3.2.

3.2 Flow Chart and Software Architecture for Implementing the Ring Test

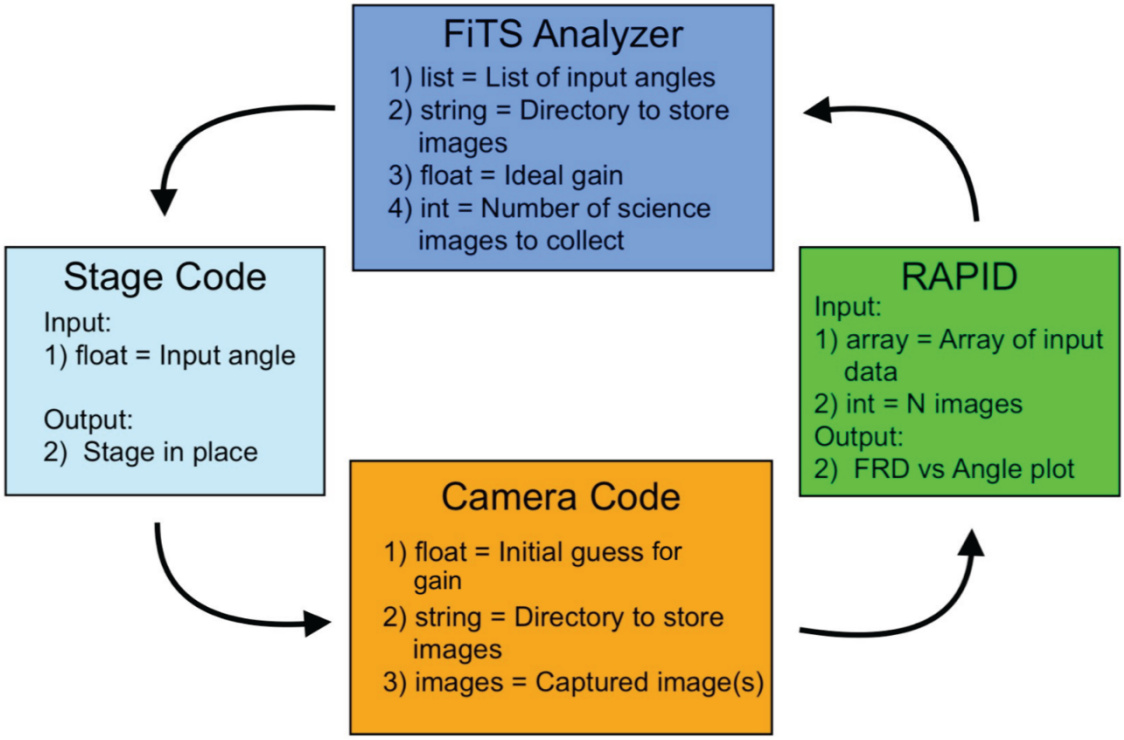

Figure 3.2: Flow chart of the Big FFW with each box pertaining to a software module.

The modules for the camera, rotating stage and image analysis are controlled by the master program, termed the “Big FiTs Fibre Wrapper”. The Big FFW is comprised of two layers: (i) the first layer was written as a graphical user interface (GUI) using the built-in Python library Tkinter, (ii) the second layer manages the various automation modules and user inputs to produce the final results. A flow chart of the Big FFW is given in Figure 3.2, with each of the automation modules shown as a block. The user input to Big FFW is simply a list of incident angles, the camera gain, the number of images to take for each angle, and managerial paths to save the output images and final results.

Camera control and adjustment were kept to a minimum by choosing to use the automatic exposure option of the FlyCapture. This decision was made after performing

tests to examine the effect of different intensities on final FRD measurements. Images were taken using the auto exposure time option at various angles and found to differ in intensity by 62% between initial and final injection angles, raising some initial concerns. Images were then collected after adjusting the exposure time by eye to match intensities between the initial and final injection angles, bringing the intensity difference down to 14%. The resulting FRD measurements between the images taken using the auto exposure time option and taken by eye (with markedly different intensities), differed by < 1%. Therefore, we propose that changes in the intensity of CCD in our system are not the dominant source of error (i.e. micro-bending or polishing problem of the fibre surface) in performing FRD measurements. Instead we attribute the dominant source of error in our system to non-homogeneities in ring illumination, which we have attempted to remove through accurate alignment and analysis routines. Additionally, the existence of a micro-lens array mounted on the face of the camera CCD introduced uneven illumination of one ring axis at large incident angles. This effect and possible solutions will be investigated further in the future but was neglected in this work as injection angles were kept below 14 degrees equivalent to f/2 (see Equation 2.3).

3.3 FRD Analysis Code for the Ring Test - RAPID

The illustration of Figure 3.3 shows how the software of the Ring Analyzer Python Interface for ring-test Data (RAPID) is presented to the user. This software examines the analysis steps of the output ring image.

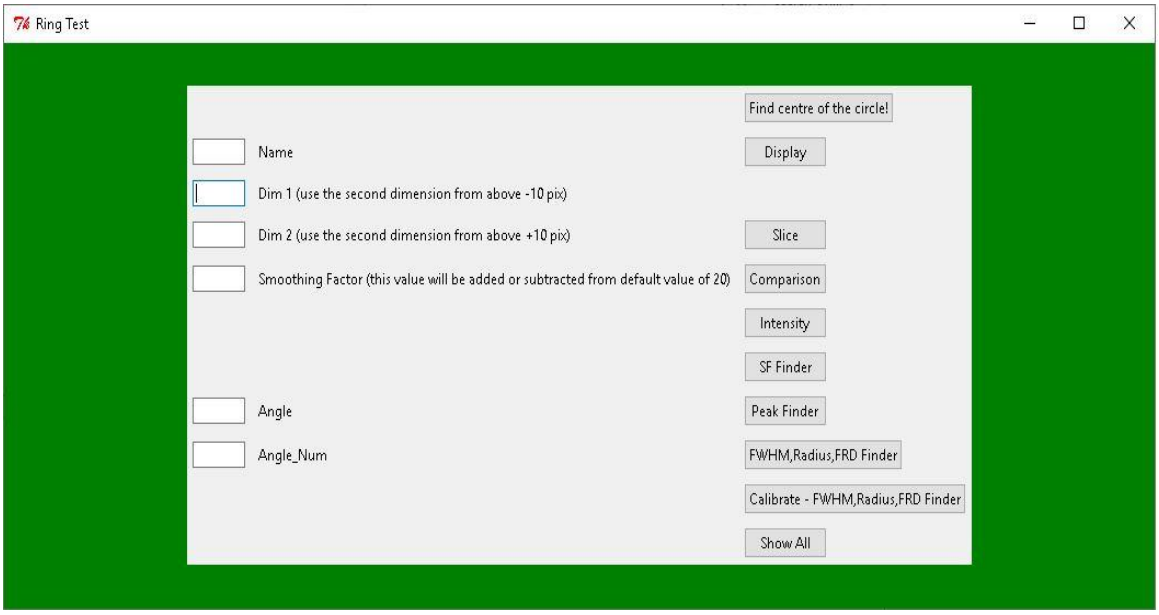

Figure 3.3: the Ring Analyzer Python Interface for ring-test Data (RAPID).

The RAPID software has several features:

1. **Find the centre of the circle:** This function will display the coordinates of the centre of the ring in pixels.
2. **Display:** Displays the input image as an original image and also as a sliced image based on the centre point of the ring image.
3. **Slice**: Plots intensity vs pixel number graph based on the chosen slice region.
4. **Comparison**: Compares the original data with the filtered version.
5. **SF Finder**: Determines the best smoothing factor by giving the mean of the difference between the smoothed graph and the original graph.
6. **Peak Finder:** It finds the maximum intensity of the plot generated from the sliced image.
7. **FWHM, Diameter, FRD Finder**: Determines the diameter of the circle (in pixels), fits a spline polynomial to the Gaussians and calculates the Full-Width Half Maximum (FWHM) and also the Focal Ratio Degradation (FRD) of the ring.

8. **Calibrate – FWHM, Radius, FRD Finder**: Rotates the image several times with random angles and determines FWHM, FRD of the images.
9. **Show All** – It determines FRD of multiple rings in multiple files, and plots a graph of FRD vs angle of all rings captured.

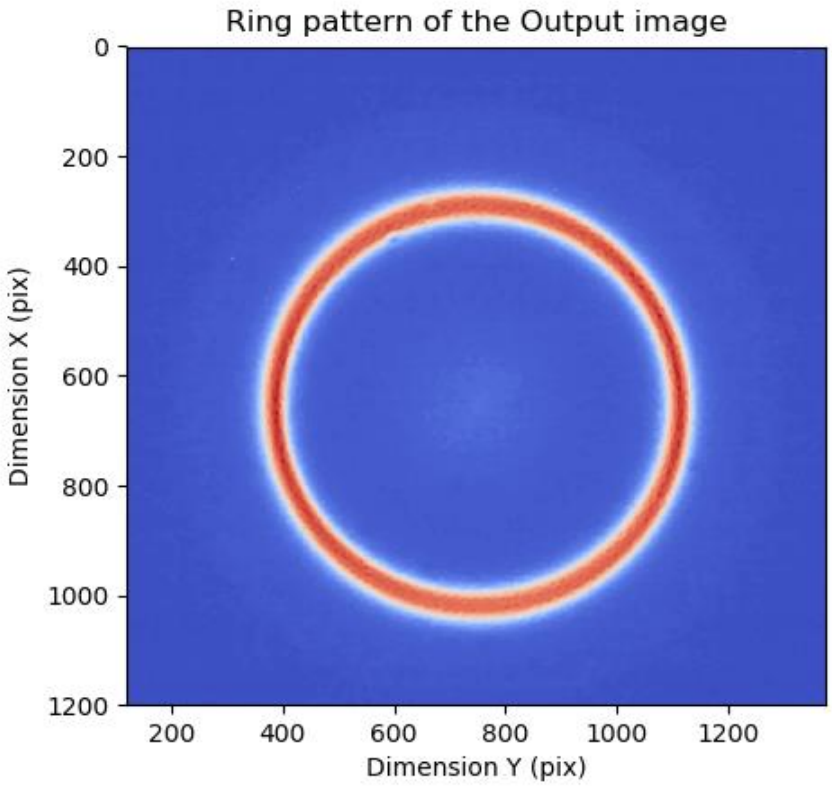

Figure 3.4: Ring-pattern image of output, using “Display” function in RAPID. The colour is scaled based on the intensity level of each pixel in the image.

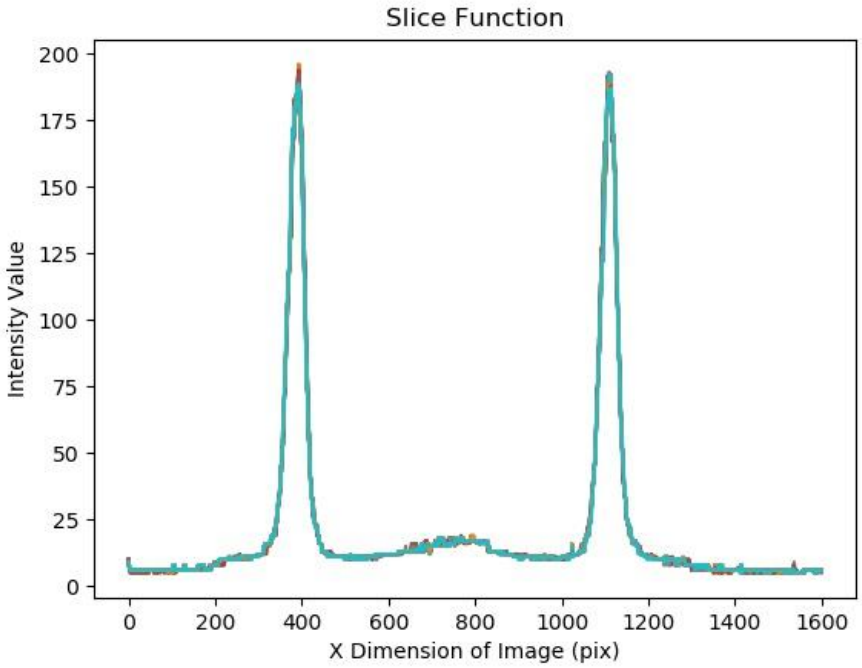

Figure 3.5: “Slice” function in RAPID. This function plots the sliced region based on the centre coordinate of the ring image.

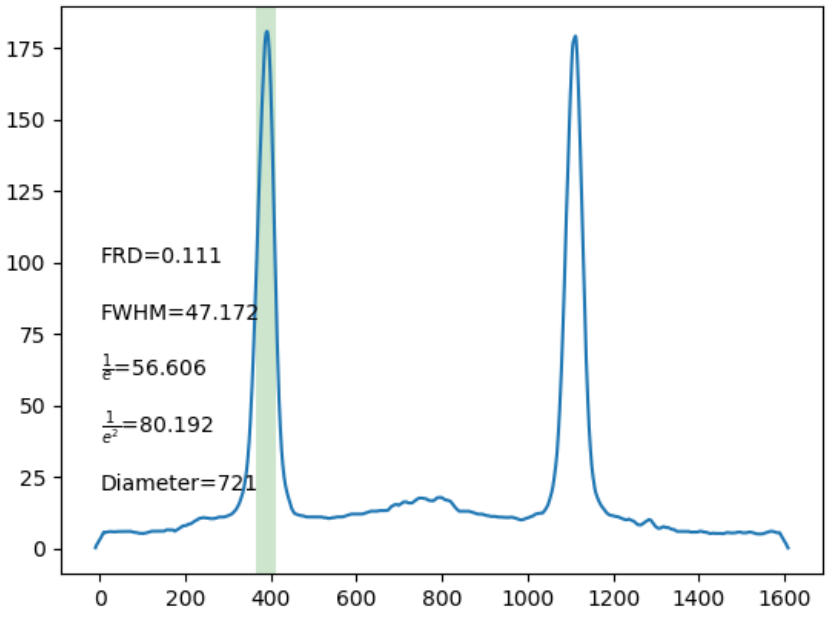

Figure 3.6: The output results of RAPID software which displays the measured values and FRD result.

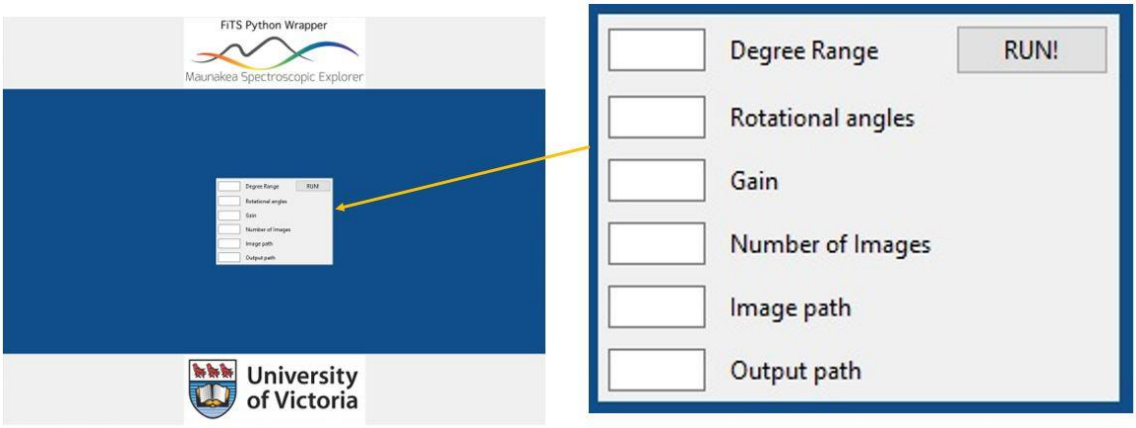

Figure 3.7: The graphic user interface (GUI) of Big_FFW.

Figure 3.7 shows the final GUI of BIG_FFW for the ring test process. The user is required to enter the incident angles, rotational angles to tilt the output image with a specific angle, a gain for the CCD and the number of images. The FRD analyzer software (RAPID) is involved as a part of the analyzing code, so the result will be shown based on the RAPID functions.

3.4 Results of the FRD Measurement

The multi-mode GRACES fibre was tested using the Big FFW on the FiTS optical bench. FRD-proxy measurements were made for 14 different incident angles (-14˚ to -8˚, and 8˚ to 14˚). -7˚ to 7˚ has no observable FRD, so these incident angles were neglected.

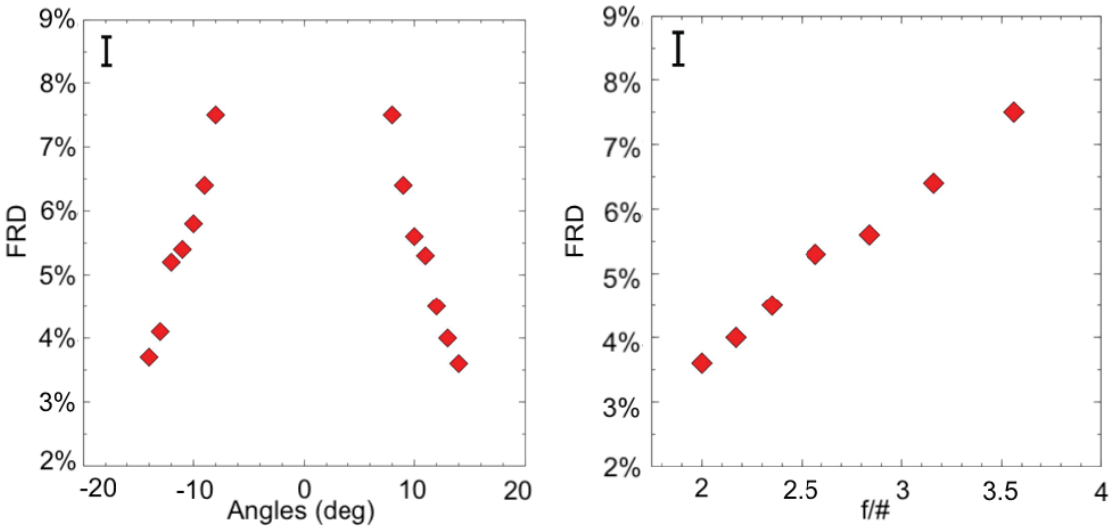

Figure 3.8: The FRD at 14 different incident angles found using the Big FFW (left panel). The symmetry in the plot suggests that our calibration process for finding the zero point has been successful. The f/# plot of the positive angles is also calculated using Equation 2.3. The right panel suggests that our estimated FRD of 3.7% at f/2 is consistent with the science requirement of the MSE project. Error bars for all data points are pictured in the left upper corner of both panels.

This result shows that we have met the science requirement of the MSE project. We have FRD of 3.7% at f-number 2. The science requirement for the MSE project requires a change of less than 5%. Furthermore, the FRD of the MSE candidate GRACES fibre was determined manually between results from the Big_FFW and the manual Ring Test to be less than the systematic error in our analysis (i.e. systematic error of 0.5%).

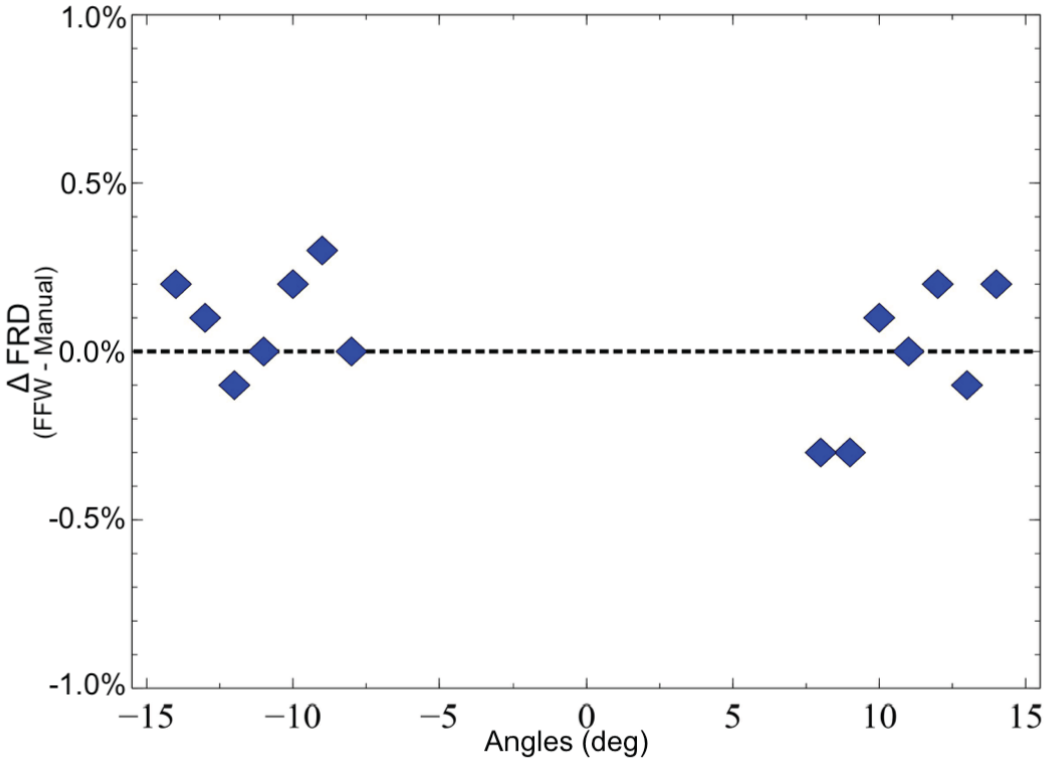

Figure 3.9: The difference between FRD values with the automated system and the manual measurement

Figure 3.9 indicates that our Big FFW is in close agreement with results from the individual/manual measurement of FRD. The maximum difference between the automated system and the manual measurement is obtained less than 0.5%.

Chapter 4 – Focal Ratio Degradation Measurement of a Multi-Mode Fibre Bundle

In the previous chapter, a technique for measuring the focal ratio degradation (FRD) of a single multi-mode fibre was presented. In the MSE FiTS, there are 57 fibre bundles with 76 multimode fibres in each bundle (3,249 fibres are for the low-medium resolution spectrographs and 1,083 are for the high-resolution spectrograph). It is critically important that every fibre in each bundle is thoroughly tested after manufacture and assembly to ensure that the optical throughput and FRD are within the stated performance specification Furthermore, this quality control operation must be achievable for each bundle within 40 hours (one-bundle-per-week production schedule). In order to develop an automated ring test measurement on 76 fibres within a bundle, a representative system was purchased from CeramOptec with the following specifications (more details can be found in the Appendix):

- A protective buffer of diameter 125 µm.
- A cladding diameter of 110 µm.
- A core diameter of 100 µm.
- The overall fibre length of 10m in length.
- Fibre numerical aperture (NA) is 0.28 ± 0.02

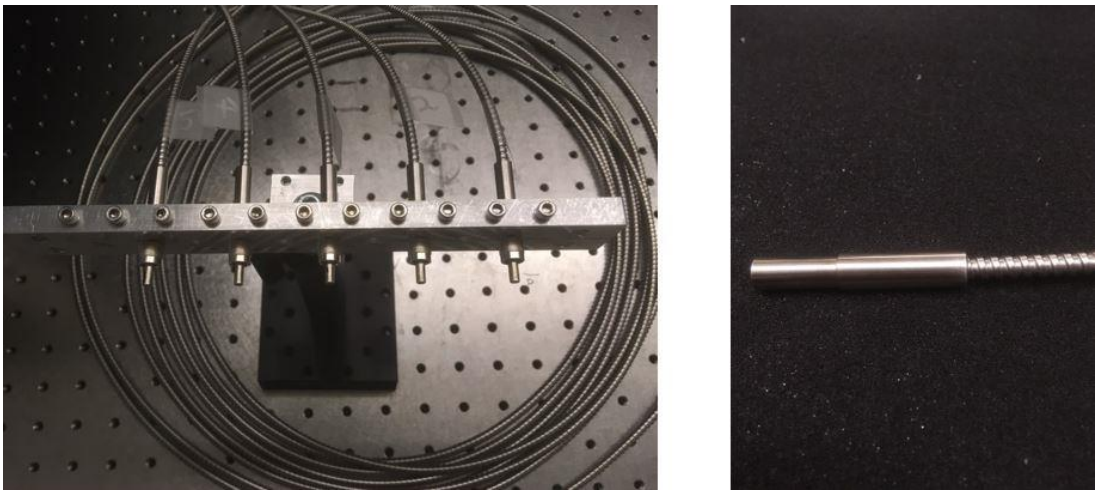

Figure 4.1: Five Individual Fibres with metallic SMA connectors (Left), and the other side of a fibre bundle with the five fibres in a small slit (Right)

As shown in the photograph of Figure 4.1, the fibre bundle consists of 5 individual fibres. On one side of the bundle there five fibres placed linearly along a small slit, see Figure 4.2. The slit has a width of 0.625mm and a height of 0.125mm. At the other end of the bundle, the five optical fibres are individually terminated with SMA connectors.

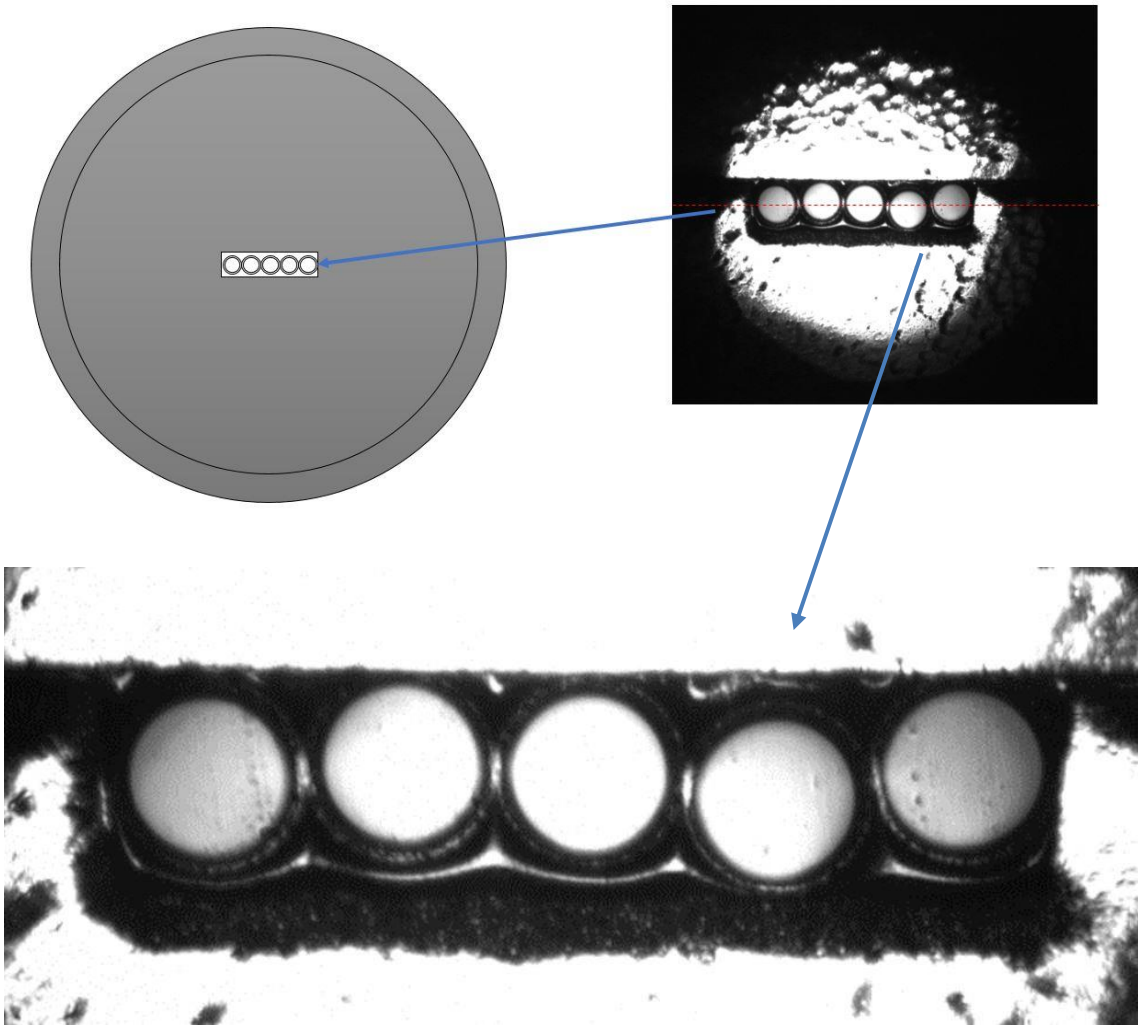

Figure 4.2: The arrangement of fibres in the small slit. The image was captured by a microscope objective with X5 magnification. It is clearly seen that the fibres are attached together without any spacing, and the vertical arrangement of the fibres is not consistent. From the left side, fibres were numbered from #1 to #5.

However, there is an issue with this fibre bundle. The fibres inside of a small slit are arranged and fixed with Epoxy glue, and glued fibres have some loss of light due to the presence of blind spots between the individual fibres. Furthermore, the fibres are touching and pressing each other. Especially, the last fibre (fibre #5 in Figure 4.2), the shape of the fibre buffer and cladding were slightly distorted because of the contact strength. This problem changes the surface flatness of the fibre and causes more FRD. However, this fibre misalignment error can be minimized by using a V-groove slit. Fibre placement with V-grooves not only reduce the error of misalignment but also allows for custom spacing between the fibres.

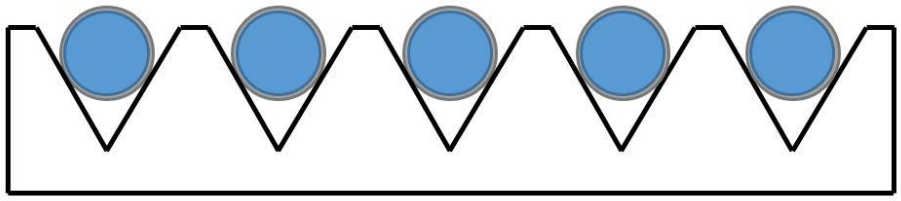

Figure 4.3: A simple schematic of the V-groove slit to minimize the alignment error.

4.1 Experimental Arrangement for Measuring FRD on a Multi-fibre Bundle

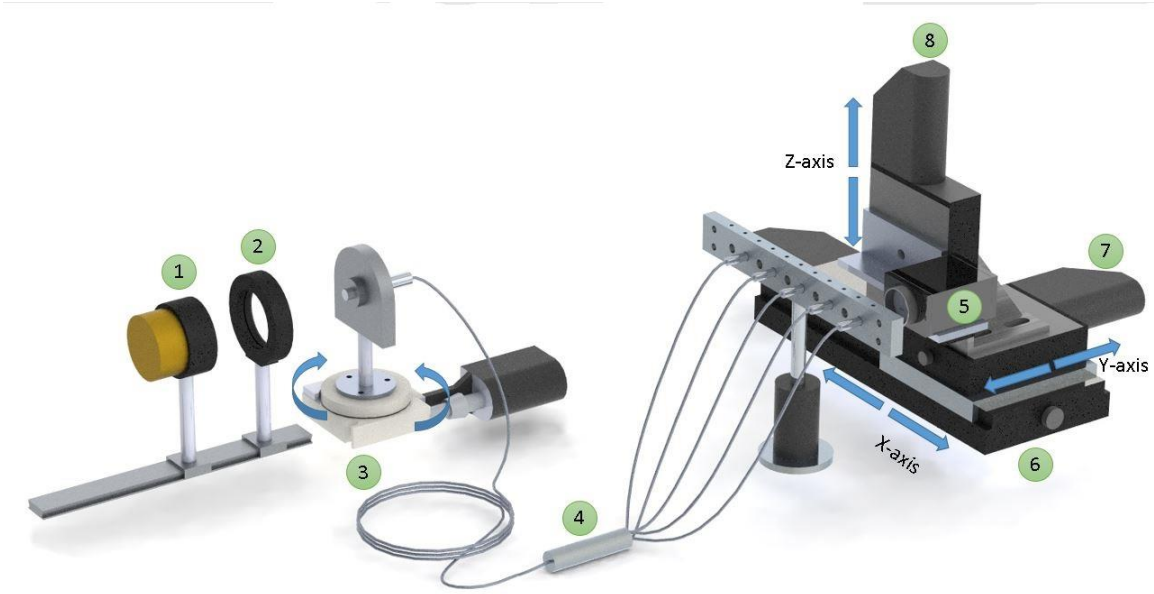

(a)

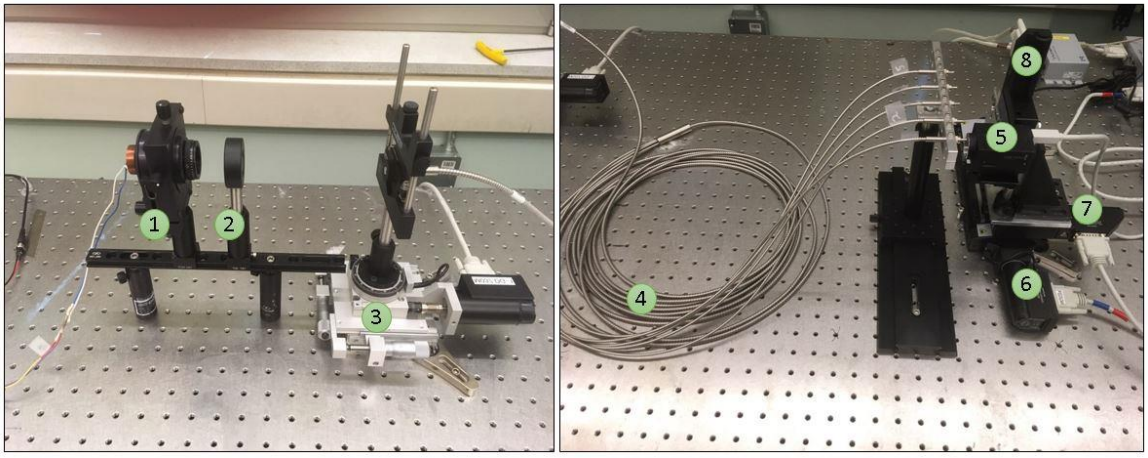

(b)

Figure 4.4: (a) A schematic diagram showing the main components of a multi-fibre FRD measurement system. (b) Photograph of the test-bed setup

The experimental setup for the FRD measurement consists of the following components:

1. Light source (#1)
    - A blue monochromatic beam at a wavelength of 460nm.
    - This wavelength is used because it is at the shortest end of the MSE measurement spectrum.
2. Collimator (#2)
    - Achromatic doublet lens with a 5cm focal length and diameter of 2.54mm.
3. A rotational stage (#3)
    - Physik Instrumente – M037.DG
4. The fibre bundle under test (#4)
5. A high resolution imaging camera (#5)
    - Point Grey, GRAS-50S5M-C with a 2448x2048 resolution (#5)
6. Linear X-axis stage with 100 mm travel (#6)
    - Physik Instrumente – M410DG
7. Linear Y-axis stage with 25 mm travel (#7)
    - Physik Instrumente – M126DG
8. Linear Z-axis stage with 25 mm travel (#8)
    - Physik Instrumente – M126DG

The linear stages have high accuracy and repeatability with a Nanoscale movement. The maximum speed is 1mm/sec and the minimum speed is 100 nm/sec. The connection time to operate the system takes 1min 30sec, and testing one single fibre takes approximately 2 minutes 30 seconds. Therefore, the total processing time to measure all 5 fibres in a bundle is approximately 13 minutes. The MSE has a one-cable-per-week production schedule for 57 cables (there are 57 fibres plus spares in each LMR cable tube; 19 fibres plus spares in each HR cable tube), and this system is able to measure all 76 fibres within 3hours 15minutes. By fully automating the metrology process, this testing system can support one cable per week production schedule.

4.2 Software Flow Chart for Automating the Experimental Apparatus

The architecture of the automation software developed for the project is illustrated in the flowchart of Figure 4.5. In the software, there are three main modes of operation:

1. **Centre positioning** – This mode defines the current position of the beam on the CCD and adjusts the 3-axes stage to position the beam at the centre of the CCD.
2. **Zero calibration** – This mode defines the normal incident angle of each fibre and corrects the angle to be 0˚
3. **FRD analysis (RAPID)** – This is a post-processing code to analyze the captured Far-field output image in order to define the FRD of each fibre.

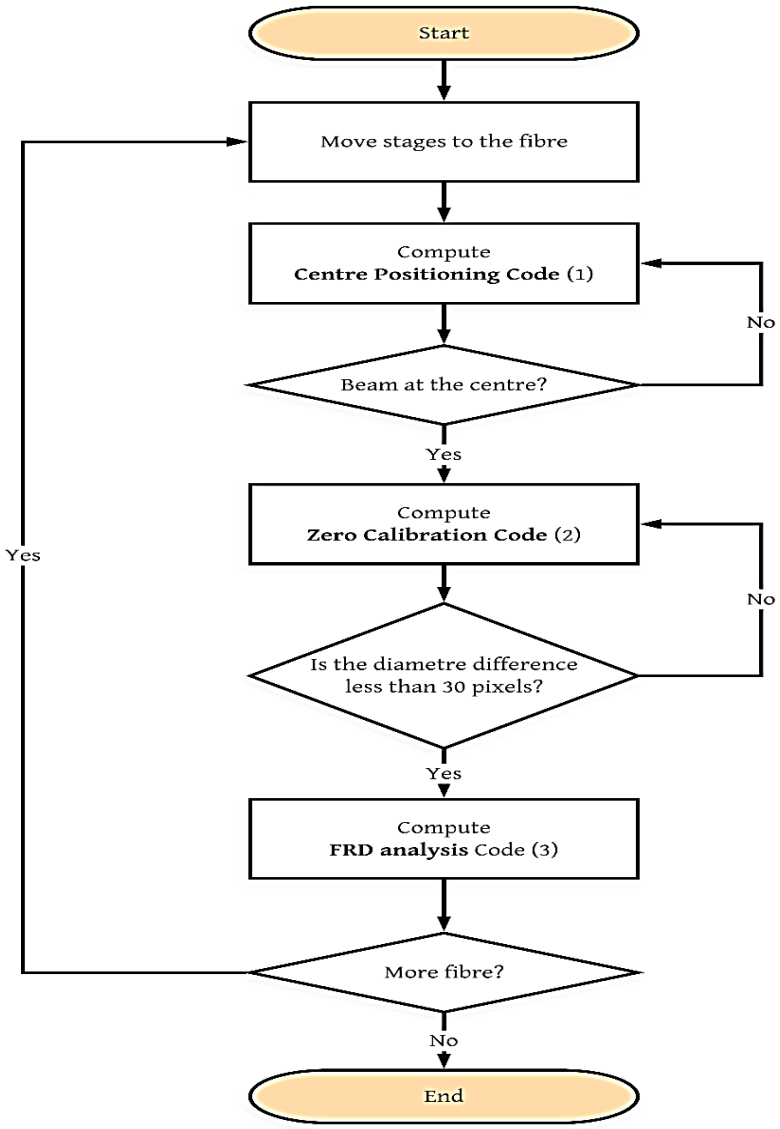

Figure 4.5: Flow chart of the multiple fibre FRD measurement

4.3 Detailed Description of Software Module Operation

4.3.1 Centre Positioning

This calibration code is used to increase the consistency of the results. It is important to repeatedly image the beam onto the same location on the camera's CCD sensor because CCD pixels can have a different sensitivity for each location. Also, if the light beam is slightly off the centre of the CCD sensor, the camera will not be able to capture the entire image of the output ring at F/2. Therefore, the code adjusts the 3-axis stage to position the output light in the exact centre of the screen. An object tracking algorithm has been developed for use in this code and defines the position of the light beam. When the camera detects the boundary of the beam, the coordinates of the current position of the beam are stored. Then, two stages (X and Z stages) are adjusted in order to bring the light to be positioned at the centre of the CCD. This process is illustrated in the sequence of images in Figure 4.6.

Before Correction

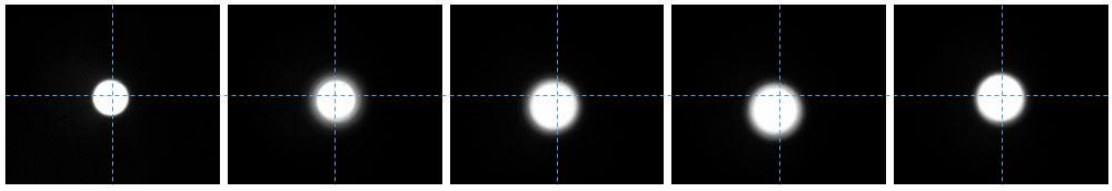

After Correction

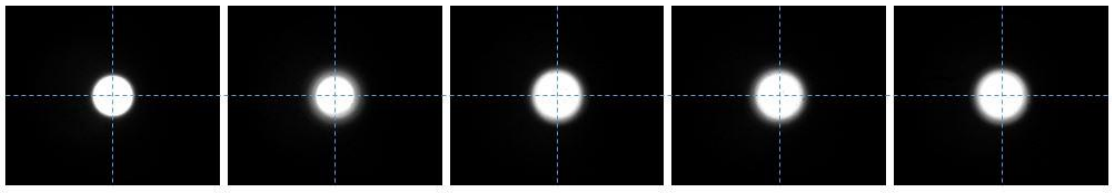

Figure 4.6: The top panel is the original position of the light before the calibration. The bottom panel indicates all beams are positioned at the centre of the CCD screen.

4.3.2 Zero Calibration

The zero calibration software process proceeds once the centre positioning process has been performed. This code finds and corrects the normal incident angle of each fibre.

The structure of the fibre assembly in the bundle's slit was examined under a microscope to determine the nature, and degree, of the fibres' spatial irregularities. After a careful examination was performed on all fibres, the nature of the two assembly deviations is characterized as:

- Linear misalignment – as shown in Figure 4.7, fibre #2, #3, and #5 are located above the centre line of the fibre #1 at about 9.34 µm, 3.16 µm, and 6.08 µm, respectively. Fibre # 4 is located 12.17 µm below the reference.

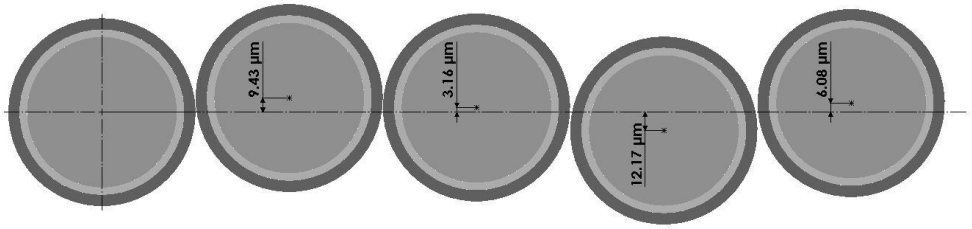

Figure 4.7: A diagram of the linear misalignment

The linear misalignment causes the total internal loss when the light is passing through the optical fibre. This loss results in a lower resolution of the fibre output FF image. However, the X-Y linear misalignment has a considerably small effect on FRD as long as the collimator is used because the collimator illuminates the light uniformly to the fibre surfaces. The FRD is affected more by the polishing and termination properties of the core surface.

- Angular-misalignment - Several fibres were physically tilted along the axis of its core during the assembly process; i.e. the axial axes of the fibres in the slit are not perfectly aligned. The angular-misalignment not only causes the loss of light but also changes the normal incident angle of the fibre. It is important to confirm that the normal incident angle of each fibre is 0˚. When the normal incident angle

is not 0˚, the fibre receives the different F/ratio light at 14˚. Therefore, the zero calibration code defines and corrects the normal incident angle of each fibre to be 0˚ so that the fibre can accommodate the correct f-ratio at each incident angle.

Before Calibration

a) Incident angle was rotated to -13˚

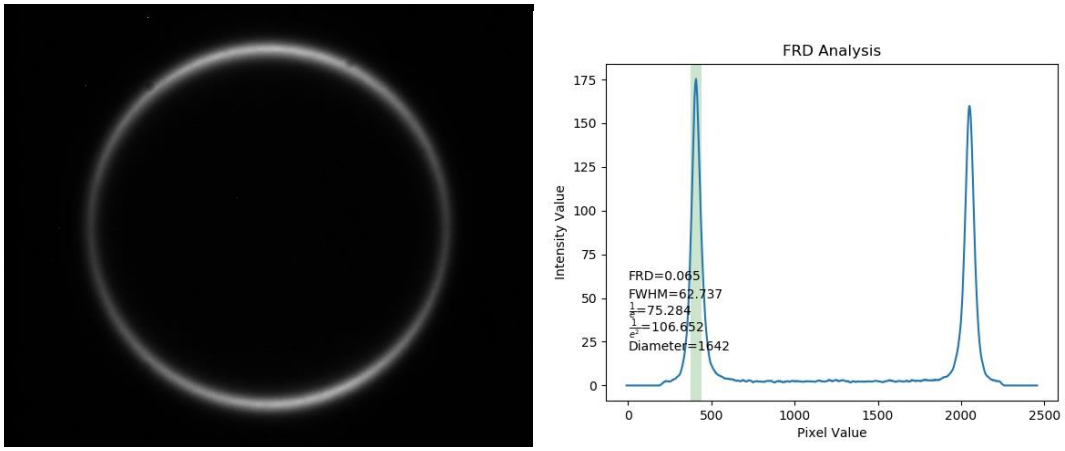

b) Incident angle was rotated to 13˚

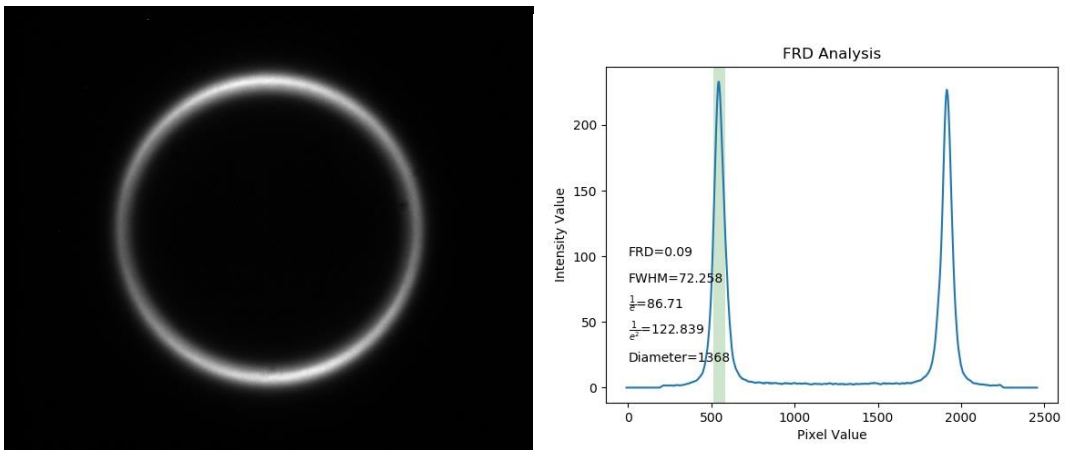

Figure 4.8: The diameter of the ring in both direction at 13˚ before calibration.

Figure 4.8 shows the FFW images in both directions at +13˚ and -13˚. The ring image at +13˚ is relatively smaller than the ring image at -13˚. The diameter of the ring at -13˚ is 1642 pixel values, and the diameter of the ring at 13˚ is 1368 pixel values. The diameter different between two ring images is 255 pixels.

After Calibration

a) Incident angle was tilted to -13˚

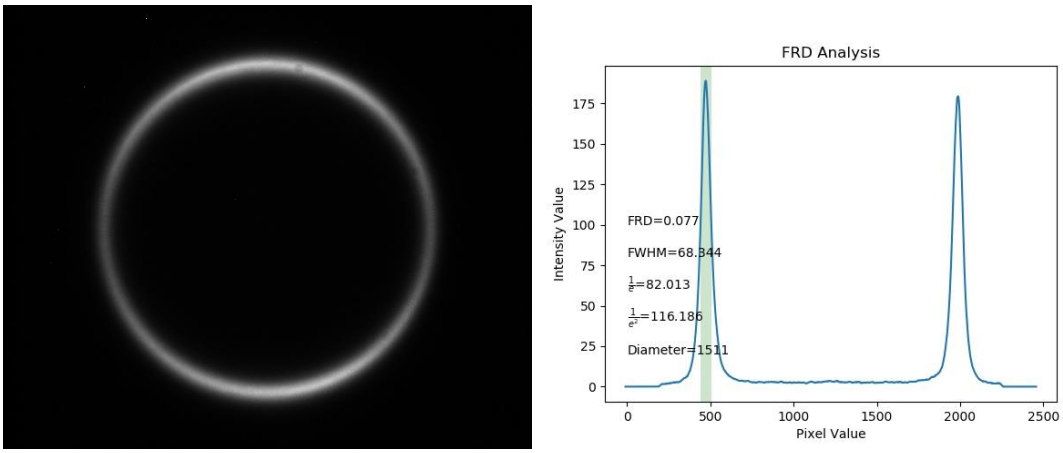

b) Incident angle was tilted to 13˚

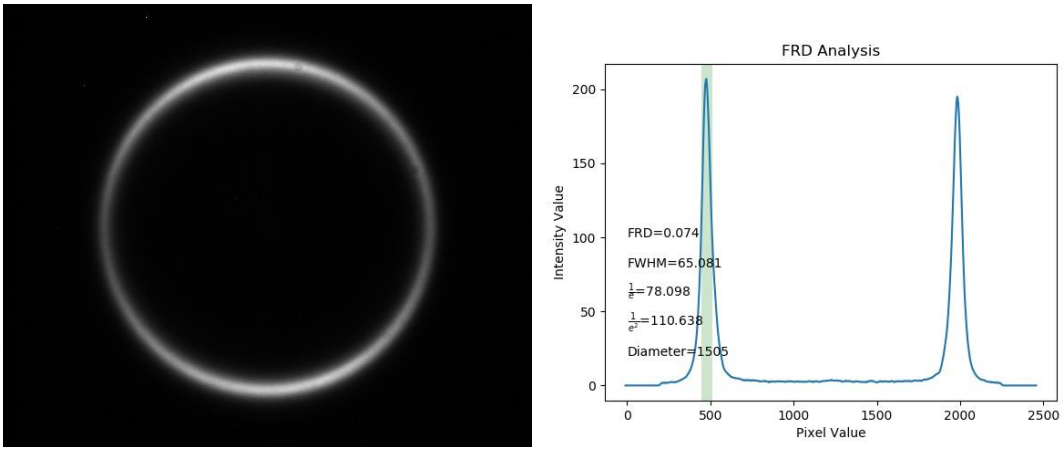

Figure 4.9: After applying a zero calibration code

After a zero calibration, two FF images at both directions have the almost same diameter. The diameter of the ring image at -13˚ was obtained 1511 pixels, and 1505 pixels at 13˚.

4.3.2.1 The methodology of the zero calibration:

This code compares the diameter of the FF output ring image captured by rotating the input of the optical fibre clockwise by 13˚, and the diameter of the ring obtained by rotating the input counter clockwise by 13˚. If the ring diameter of one side is larger or smaller than the other, it means the normal incident angle of the fibre is tilted. It is important to find the difference in diameter of the two captured images and to adjust the input angle so that the normal incident angle is zero. For calibrating the normal incident angle, it is necessary to determine how the diameter of the ring varies with the angle of incidence. From Figure 4.10, it can be seen that the ring diameter increases constantly from 4˚ to 14˚. However, from 0˚ to 3˚, there are no observable changes in diameter, so they are neglected when the increment of the diameter was estimated. When the incident angle changes by 1˚, the diameter output ring image increases constantly by about 110 pixels.

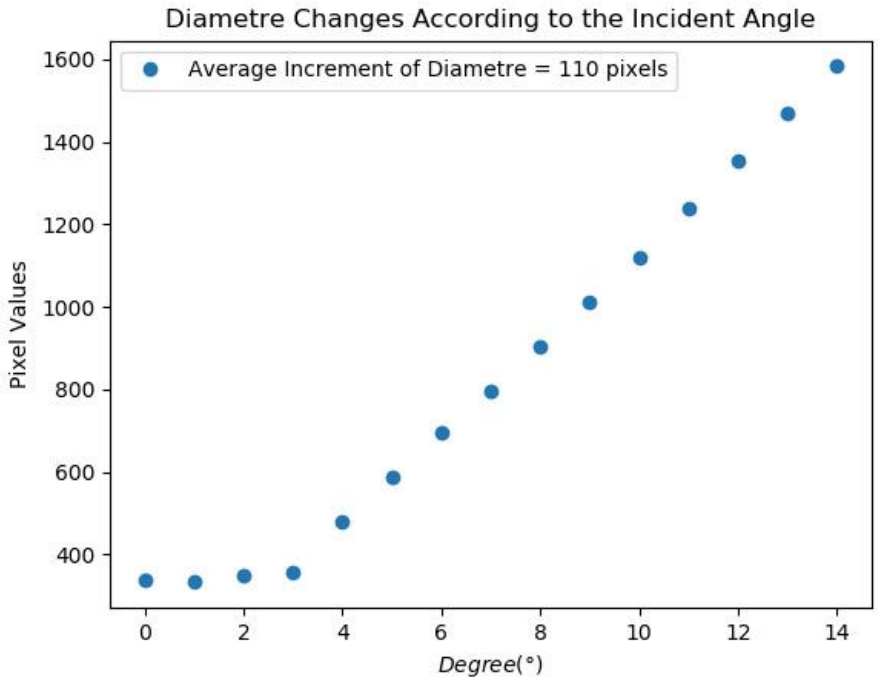

Figure 4.10: Diameter change of fibre output image based on the different incident angle.

4.4 Results of FRD measurements on the fibre bundle.

The focal ratio degradation measurements (ring tests) were performed at two different wavelengths, using two separate light sources:

- A blue light emitting diode (LED) operating at 460 nm. (LZ1-x0DB00, LED Engine Inc.)
- A red light emitting diode (LED) operating at 625 nm. (M625L4, Thorlabs Inc.)

The FRD measurements were performed at these two distinct wavelengths in order to assess the effect of wavelength dependencies in this test. This is ultimately important for the MSE project where the targets' signal will span a spectrum of wavelengths.

FRD measurements of fibre bundles were performed 5 times at 30-minute intervals for consistency of the system. During the FRD measurements, the apparatus including a point grey camera and LED light source is heated. Therefore, we measured FRD measurement repeatedly with 30minute intervals to check the stability of the system at room temperature. As a consequence, the FRD results indicate that there is no significant change in FRD during this experiment (less than 0.3%). However, the temperature dependence of optical fibres was investigated by many researchers that there is no direct evidence of FRD occurs because of the temperature gradients, but it was found there is considerably small FRD occurs at cryogenic temperature (77K) [17],[18].

4.4.1 FRD Results of the Fibre Bundle Using the Blue LED (λ = 460 nm).

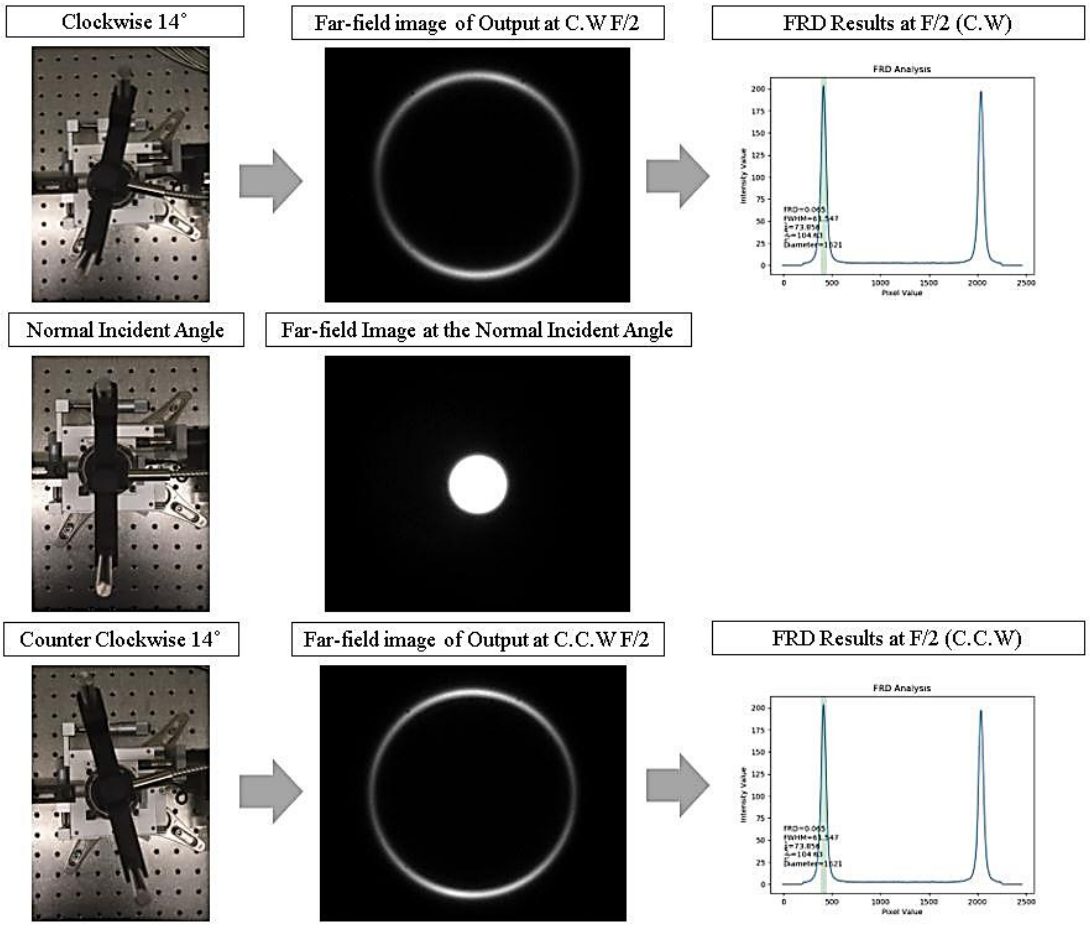

Figure 4.11: The process of FRD measurement

Table 1: FRD measurement results at bidirectional F/2 points using the blue LED (λ = 460nm)

Blue LED (460 nm)										
FRD at F/2 (%)	Fibre1		Fibre2		Fibre3		Fibre4		Fibre5	
	CCW	CW	CCW	CW	CCW	CW	CCW	CW	CCW	CW
trial#1	6.5	6.8	8.3	7.8	8.1	8.5	7.0	7.1	7.2	7.5
trial#2	6.7	6.7	8.4	7.8	8.1	8.4	7.0	7.1	7.2	7.5
trial#3	6.6	6.7	8.5	7.8	8.1	8.4	7.0	7.0	7.2	7.5
trial#4	6.6	6.8	8.3	7.8	8.2	8.4	7.1	7.0	7.2	7.4
trial#5	6.8	6.7	8.5	7.7	8.2	8.2	7.0	7.1	7.3	7.5

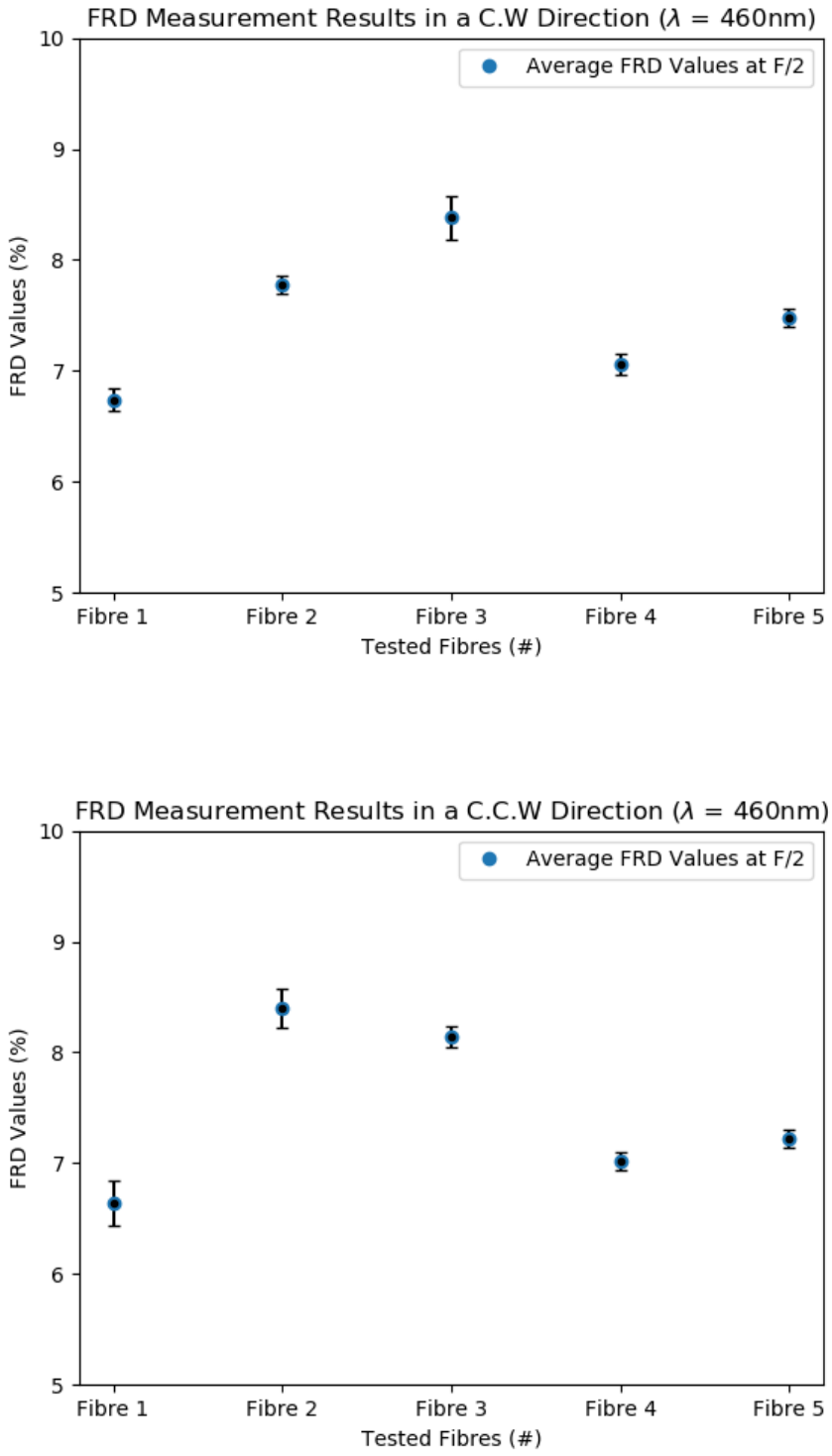

Figure 4.12: FRD results of each fibre in a clockwise direction (top), and counterclockwise direction (bottom) when the wavelength is 460 nm. Note that the error bar indicates 95% confidence intervals.

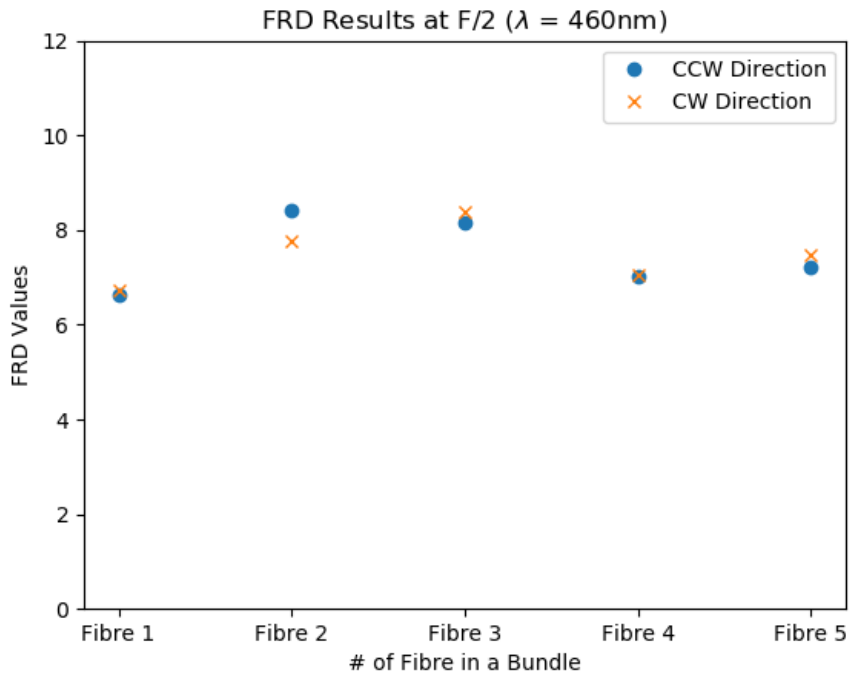

Figure 4.13: FRD results at F/2 beam in both directions.

- The FRD result range for each fibre was measured from 6.5% to 8.5%.
- The minimum value of FRD was measured as 6.6% on average in fibre #1.
- The maximum value of FRD was measured as 8.4% on average in fibre #3.

4.4.2 FRD Results of the Fibre Bundle Using the Red LED (λ = 625 nm).

Table 2: FRD measurement results at bidirectional F/2 points using the red LED (λ = 625 nm)

Red LED (625 nm)										
FRD at F/2 (%)	Fibre1		Fibre2		Fibre3		Fibre4		Fibre5	
	CCW	CW	CCW	CW	CCW	CW	CCW	CW	CCW	CW
trial#1	7.7	7.5	9.1	9.2	9.1	9.5	8.2	8.0	7.9	8.4
trial#2	7.6	7.6	9.2	8.8	9.2	9.6	8.1	7.9	8.0	8.3
trial#3	7.5	7.4	8.9	8.7	8.9	9.5	8.2	7.8	7.8	8.3
trial#4	7.5	7.3	8.8	8.8	9.0	9.2	7.9	7.8	8.0	8.3
trial#5	7.5	7.4	9.0	8.8	9.0	9.3	8.1	7.9	8.0	8.3

FRD measurements at other wavelengths (625 nm) were performed without any rearrangement of the optical bench setup except replacing the light source. For the data reduction consistency, the overall intensity of the red light output image has been adjusted to have a peak level similar to the intensity of the blue light in the camera. The measurements are a repeatable and experimental error is estimated ~1%. The overall FRD of using a higher wavelength was increased by about 0.8~1%.

- These results show the relationship between the wavelength of the light and FRD of fibres. The longer wavelength will increase the FRD.
- This effect was investigated by many different researchers. A decrease in FRD in the blue is predicted by Gloge [13] and has been observed by a number of researchers (Pazder, John [8], Carrasco & Parry [9], Poppett & Allington-Smith [12])

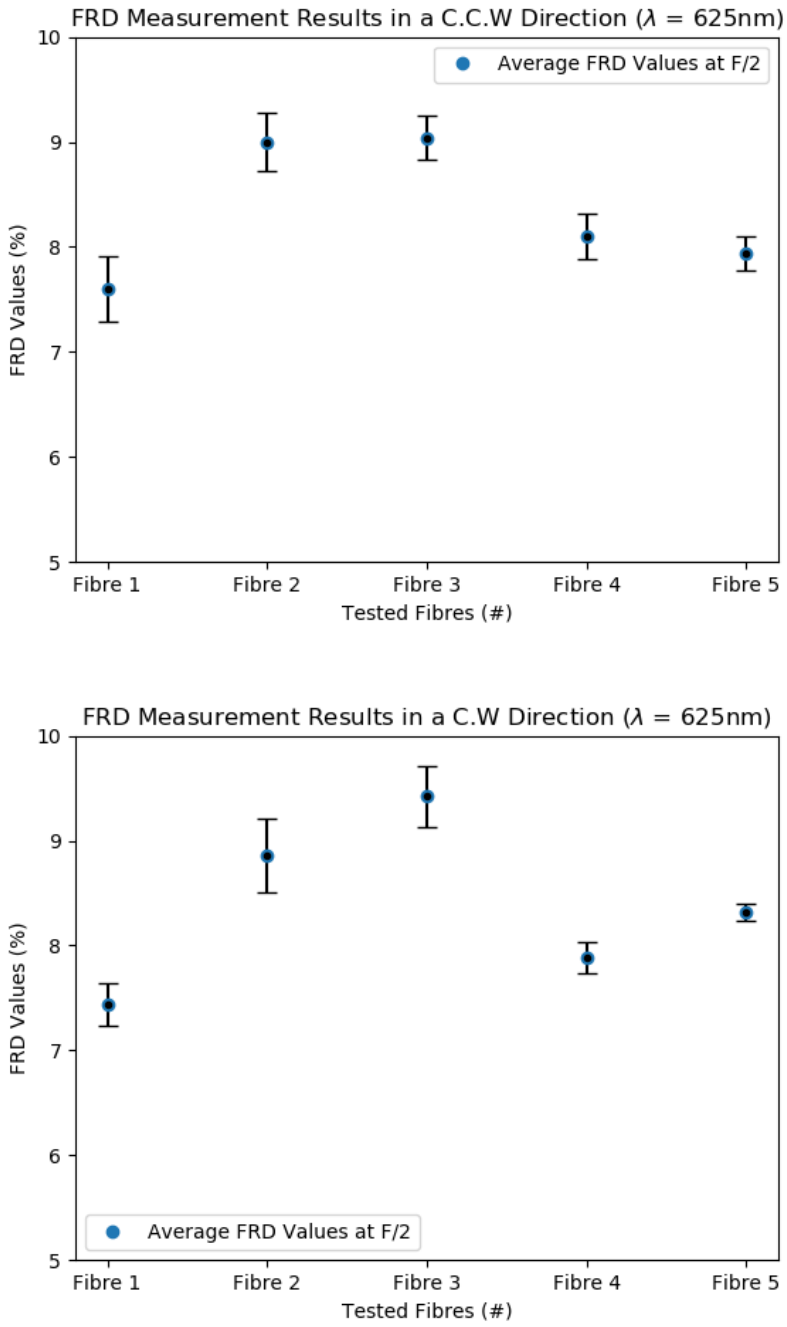

Figure 4.14: FRD results of each fibre in a clockwise direction (top), and counter clockwise direction (bottom) when λ = 625nm. Note that the error bar indicates 95% confidence intervals.

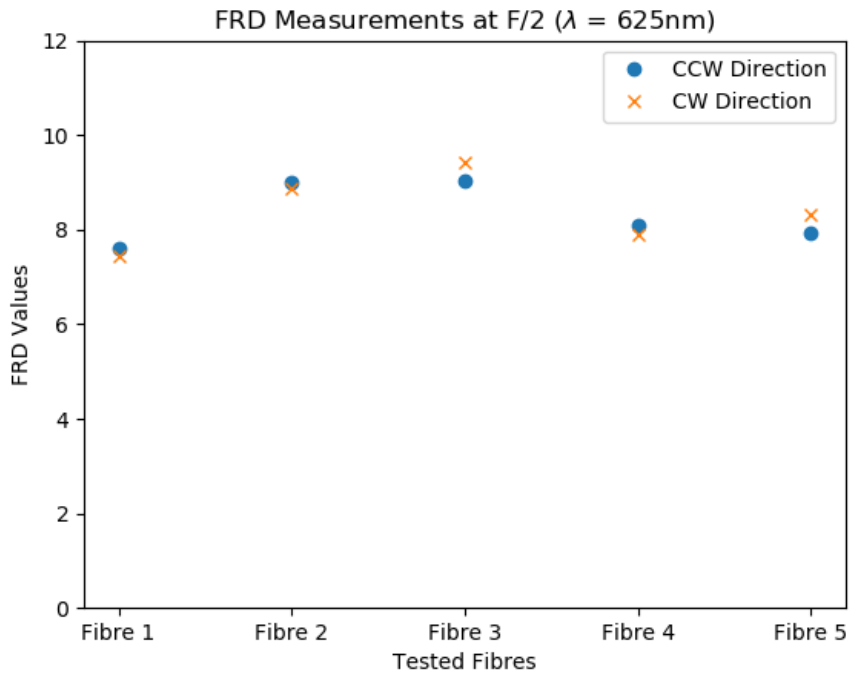

Figure 4.15: FRD results at F/2 beam in both directions

- The FRD result range for each fibre was measured from 7.3% to 9.6%.
- The minimum value of FRD was measured as 7.4% on average in fibre #1.
- The maximum value of FRD was measured as 9.4% on average in fibre #3.

Chapter 5 – MSE Fibre Throughput Measurement

The transmission efficiency of the selected MSE optical fibres is another important factor in ensuring adherence to science specifications. The efficiency of the optical fibre depends on the length of the fibre, the level of stress applied to the fibre (e.g. a tight bending radius) and environmental conditions.

In this chapter, another optical bench system has been designed to measure the amount of light entering and exiting a given length of optical fibre. By comparing the amount of input and output light, the transmission efficiency of the fibre can be determined.

5.1 Experimental Setup for the Throughput Measurement of a Multi-mode Fibre

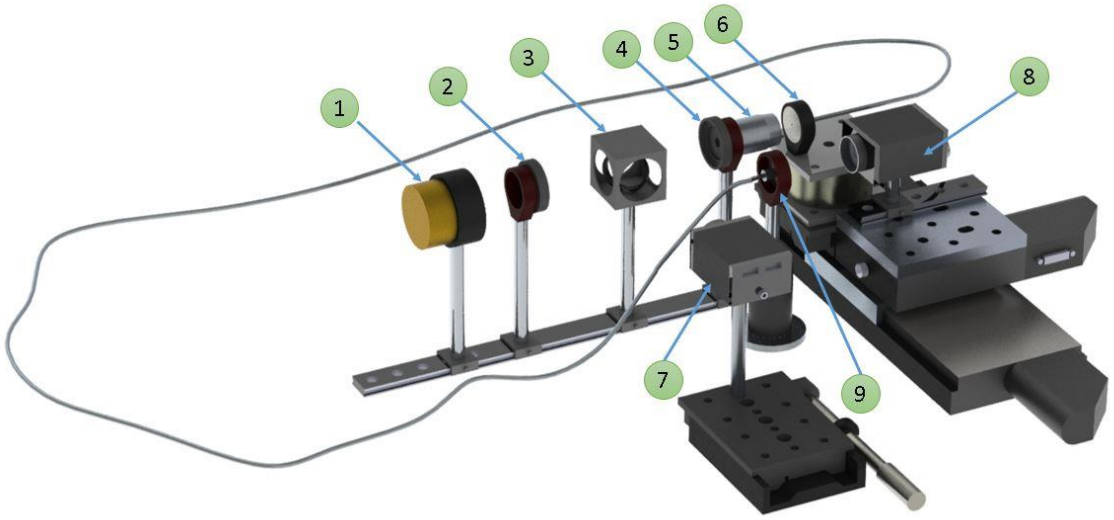

(a)

(b)

Figure 5.1: (a) A schematic diagram of the experimental arrangement used for measuring fibre throughput. (b) Photograph of the test-bed setup.

With reference to Figure 5.1, the experimental setup for measuring the throughput on the same GRACES fibre used in the FRD measurement consists of the following components:

1. Light source (#1)
    - A blue monochromatic beam at a wavelength of 460nm.
    - This wavelength is used because it is at the shortest end of the MSE measurement spectrum.
2. Field stop iris (#2)
    - A ring-actuated iris (SM1D12C, Thorlabs Inc.) that is used to adjust the size of the object.
3. Beam splitter (#3)
    - A Pellicle beam splitter, uncoated with a 8:92 (Reflection: Transmission) ratio.

4. Aperture stop iris (#4)
    - A ring-actuated iris (SM1D12C, Thorlabs Inc.) that is used to adjust the beam focal ratio entering the fibre core.
5. Microscope objective (#5)
    - A 10X magnification objective (Fisher Scientific) that focuses all of the input light beam into the core of the fibre (#6) (no light enters the cladding).
6. Light input position monitoring camera (#7)
    - Point Grey, GRAS-50S5M-C with a 2448x2048 CCD resolution.
    - The camera ensures that all input light is focused on the core.
7. Light input and output measuring camera (#8)
    - Point Grey, GRAS-50S5M-C with a 2448x2048 CCD resolution.
    - The camera can be positioned on the linear stage (100mm travel, Physik Instrumente - M410DG) to measure the amount of light entering and exiting the fibre (#9).

To measure the throughput, the point grey camera (#8 in Figure 5.1) is used to capture the input light from the microscope objective and the output light from the fibre end. The camera is mounted on the linear stage and moved to the input end or output end of the fibre to capture the far-field image of the input and output of the fibre. The pellicle beam splitter (#3 in Figure 5.1) is placed between the LED source and the microscope objective to separate the light into 92% transmittance and 8% reflectance. Another point grey camera (#7 in Figure 5.1) is used to ensure the alignment of the beam onto the fibre core surface by using the beam splitter arrangement to reproduce the image of the fibre surface, on the camera's CCD sensor, through the back reflection of light from the fibre core (as shown in Figure 5.2).

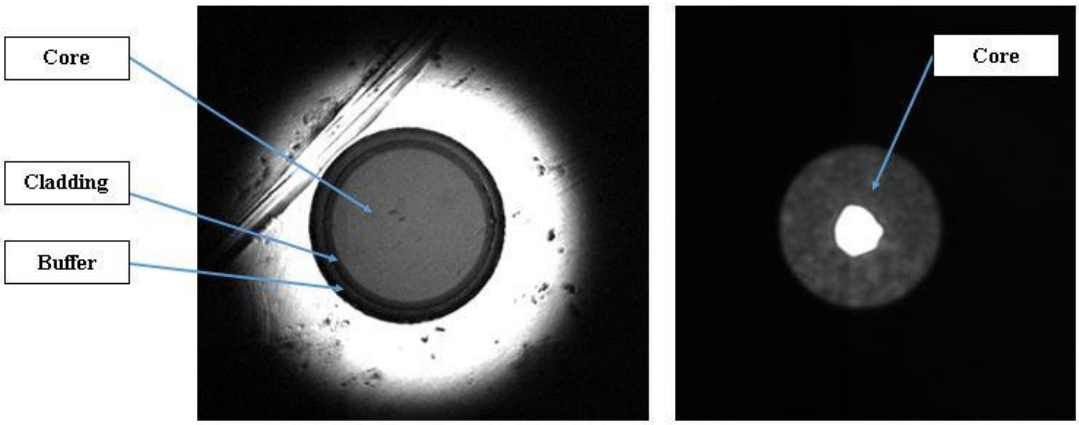

Figure 5.2: The image of the fibre surface using the 10X microscope objectives (Left), and the focused input beam on the fibre core (Right).

Two different methods have been used to measure the transmission efficiency of the optical fibre: (i) Comparing the total intensity of the input and output images captured by CCD in a given time period. (ii) Comparing the total input and output beam power using a calibrated power meter.

5.2 Throughput Measurement of Optical Fibre: Intensity comparison of input and output images.

This method uses a CCD camera to capture the direct beam of input and output, then compare the overall intensity of images. The CCD (#8 in Figure 5.1) slides into view of the incoming beam to capture the direct beam of input, and then, this camera slides back into the position of output to capture the output beam. The important thing is that the CCD camera has a limitation to measure the intensity level. The camera can only measure the intensity level of pixels up to 255. Therefore, the intensity of the light should be adjusted to have the maximum intensity value less than 255. This can be done by adjusting the power of the light source or change the properties of the CCD camera (i.e. gain and exposure time). Figure 5.3 shows the FF images obtained from the camera at each position: 1) A fibre core image with a focused beam. 2) An input image of the beam from the microscope objective. 3) A far-field fibre output image.

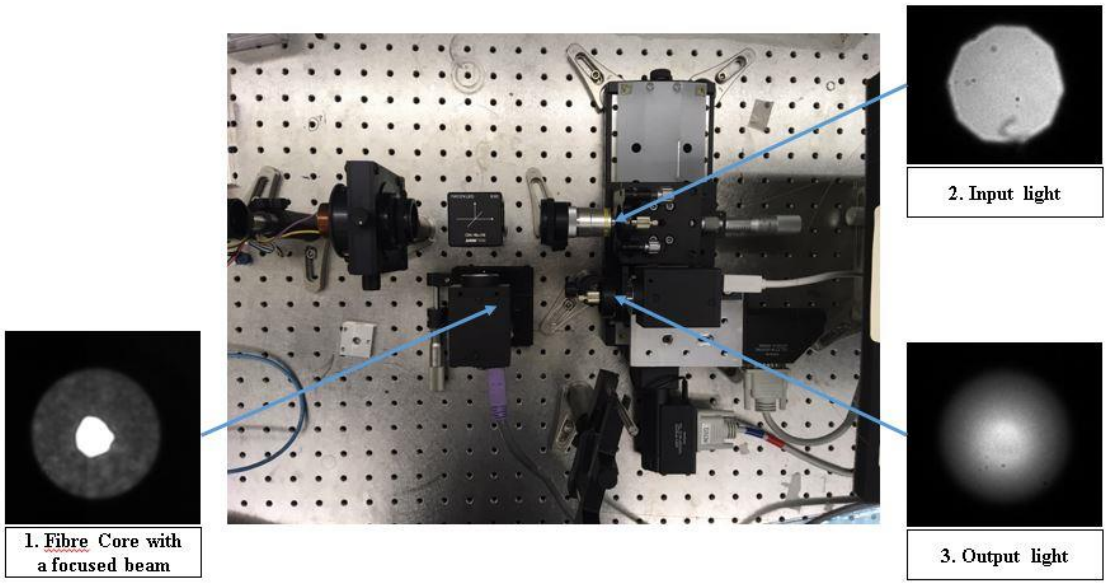

Figure 5.3: Far-field images of input, output and fibre core.

5.2.1 Image Processing of a Raw Data

Before comparing the overall intensity of input and output images, image processing is required to reduce any unwanted data. A raw image contains the data of the object, but it also includes a few imperfections such as noise, dark current, and hot pixels. To reduce or correct these imperfections, the standard procedure was used to calibrate the raw image for dark current, bias, and sensitivity variations.

There are three different images made to correct raw images:

1. Dark Frame: Dark frame is used to remove dark signals from the light frame with the CCD camera because CCD camera generates a dark signal depending on the exposure time and temperature
2. Bias Frame: Bias frame is used to remove the CCD chip readout signal from the light frame.
3. Flat frame: Flat frame is used to correct the uneven field illumination created by dust or smudges in the optical train.

The image processing steps follow:

1. Capture at least 200 images of dark, bias and flat images and create each single master image using each mean value of pixels.
2. Capture the image of input (the light from the microscope objective lens) and output (the light from the fibre end)
3. Correct both input and output images with a master dark, bias, and flat image.
4. Measure the overall intensity of corrected images
5. Calculate the transmission efficiency by a total intensity of Output/Input

Theoretical calibrating algorithm:

$$Corrected\ image = \frac{(Raw\ image - Dark - Bias)}{(flatframe)} \qquad (5.1)$$

5.2.2 Results of Throughput Measurement Using the CCD Camera.

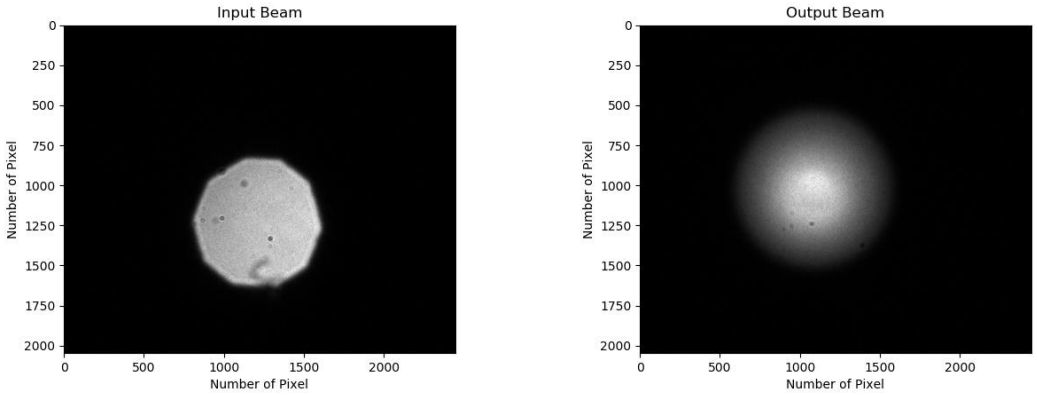

Figure 5.4: Input corrected image (Left) and output corrected image (Right)

The total intensity of both captured input and output was compared in order to define the transmission efficiency.

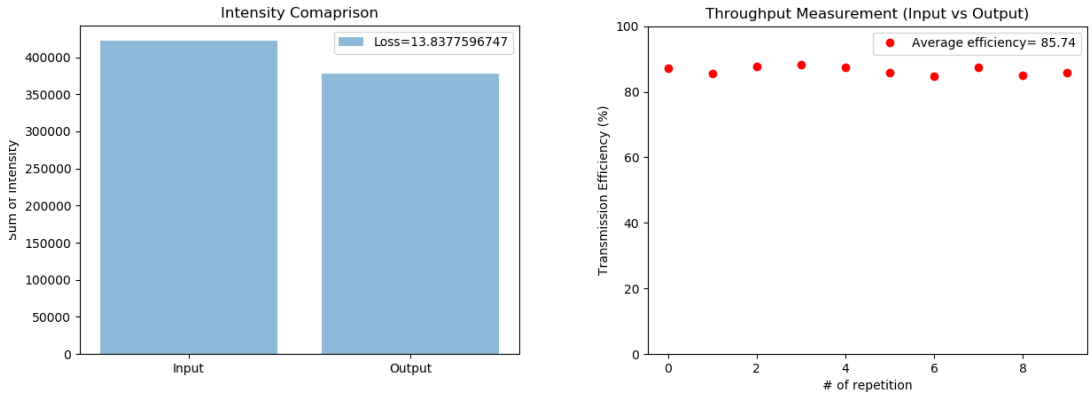

Figure 5.5: The result of throughput measurement by intensity comparison (measured 10 times repeatedly).

The average transmission efficiency of optical fibre using 460nm wavelength LED is about 86% including the Fresnel reflection loss. Fresnel reflection is the loss that a small portion of the incident light is reflected back into the light source. Fresnel reflection occurs at the interface at entrance and exit ends of an optical fibre. The ratio (R), shown below, approximates the portion of incident light (light of normal incidence) that is reflected back into the source.

$$R = \left(\frac{n_1 - n_0}{n_1 + n_0}\right)^2 \qquad (5.2)$$

Where the n_1 is the refractive index of the fibre core and n_0 is the refractive index of the medium. There is a light reflection at the end of the optical fibre, so we can monitor the fibre core image. However, it also means that there is a reflection loss from the fibre core surface. Therefore, the input light from the microscope objective is actually not the same as the actual amount of light entering the fibre core. The refractive index of the silica based fibre is 1.46 at 460nm wavelength, and the refractive index of the medium is 1.00 (air). Therefore, the Fresnel reflection loss of silica based fibre is obtained about ~3.5% at each interface. The final transmission efficiency of the fibre excluding a Fresnel reflection loss is about 93%.

5.2.3 Throughput Measurement Comparison with the Power Meter

This measurement was performed with the same settings as in Figure 5.1 except for the CCD camera. The CCD was replaced with a Newport 1380-C power meter to measure the power of the light at the input and output of the fibre.

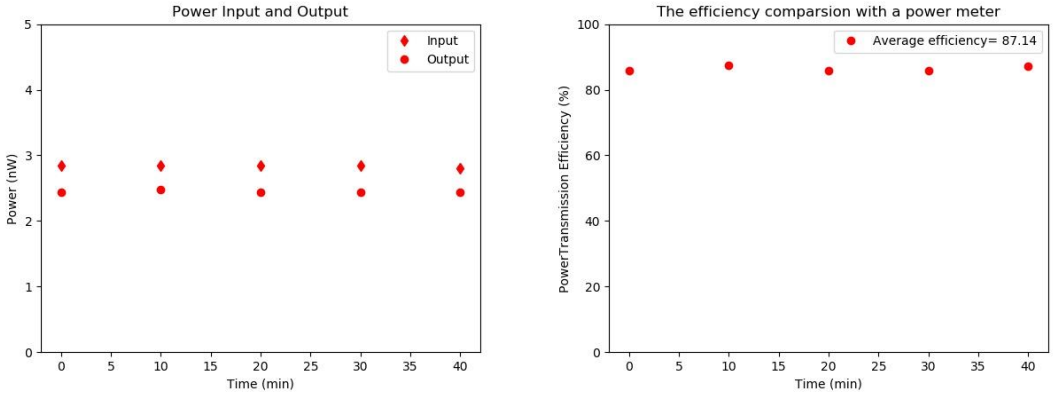

Figure 5.6: Power of the light at input and output of the fibre (Left), and transmission efficiency of the fibre (Right) including the Fresnel reflection loss

The transmission efficiency measurement of the fibre was similar to that of the CCD camera. The average efficiency measured using a power meter was approximately 94% while the efficiency measured with the CCD camera technique was 93% (excluding the Fresnel reflection loss).

5.3 Throughput Measurement of Optical Fibre Bundle: Intensity Comparison of Input and Output Images

In this section, the throughput measurement of the fibre bundle was performed. The experiment setup is the same as the pre-test with GRACES fibre as shown in Figure 5.1. This experiment also measured the transmission efficiency by comparing the total amount of intensity of the input and output images through the CCD camera and measuring the power of light through the power meter.

5.3.1 Results of Throughput Measurement Using the CCD Camera (λ = 460 nm)

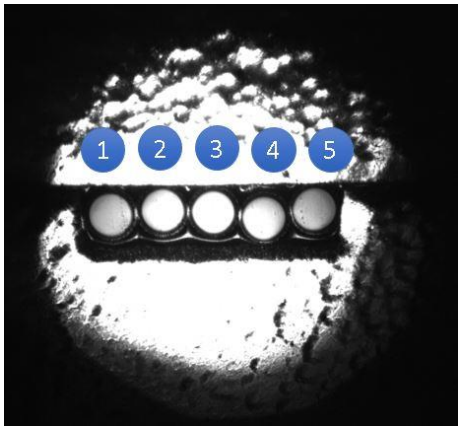

Figure 5.7: Fiber placement and numbering in a slit

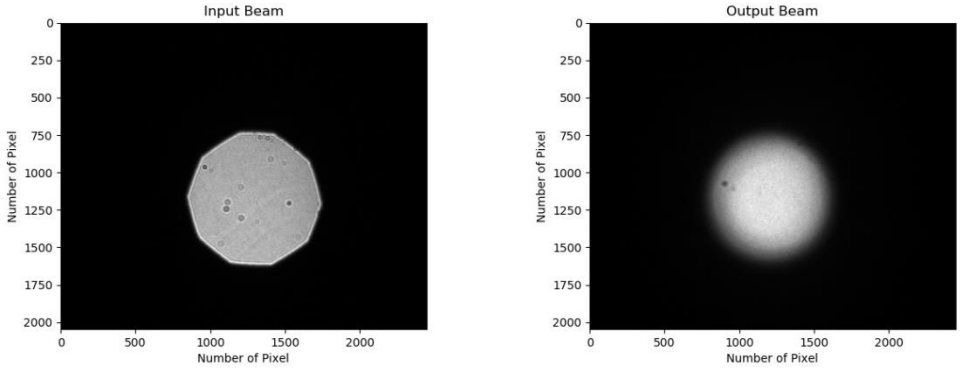

Figure 5.8: Input corrected image (Left), and output corrected image of fibre #1 (Right)

The average transmission efficiency of each fibre in a bundle was obtained:

Table 3: The results of throughput measurement of each fibre through the intensity comparison of input and output far-field images.

	Fibre #1	**Fibre #2**	**Fibre #3**	**Fibre #4**	**Fibre #5**
Transmission Efficiency (%)	96.97	97.13	96.33	95.26	94.04

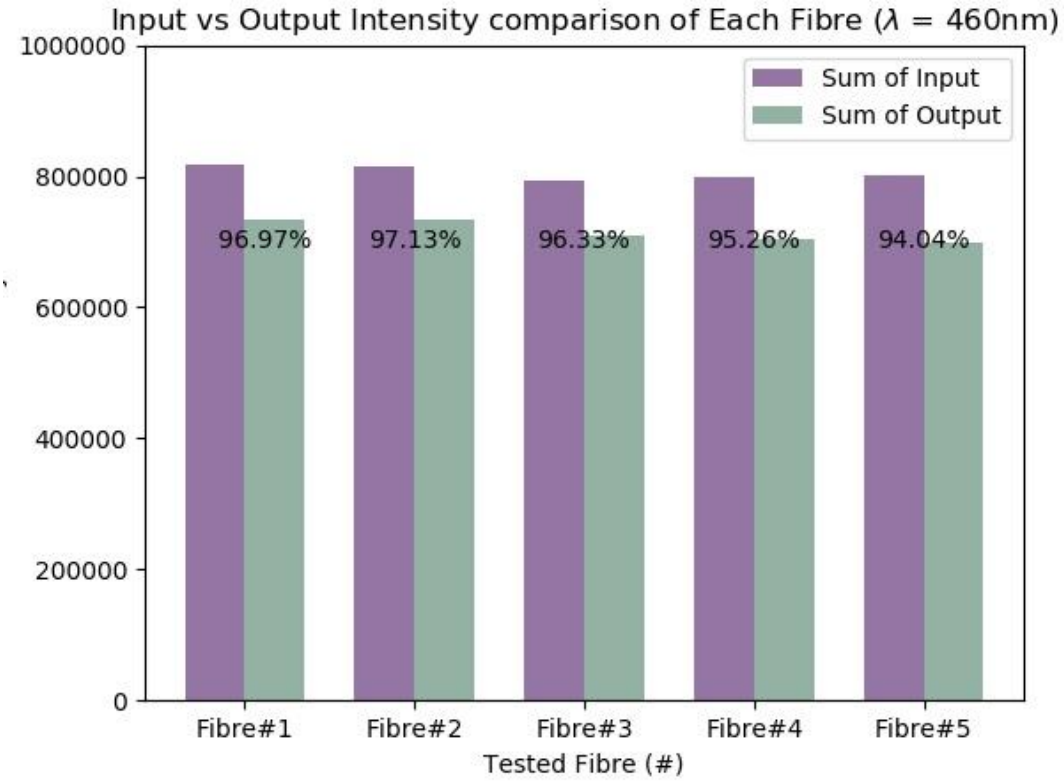

Figure 5.9: Throughput measurement of each fibre using CCD. The text indicates the transmission efficiency of the fibres. (The results exclude the Fresnel reflection loss).

The transmission efficiency range of all five fibres was obtained between 94% and 97.1%. From the result of throughput measurement using the CCD camera, Fibre # 2 has the highest transmission efficiency and Fibre # 5 has the lowest transmission efficiency.

5.3.2 Results of Throughput Measurement Using the Power Meter (λ = 460 nm).

Table 4: The results of throughput measurement of each fibre through input and output power comparison.

Throughput (%)	Fibre#1		Fibre#2		Fibre#3		Fibre#4		Fibre#5	
	Input (µW)	Output (µW)	Input (µW)	Output (µW)	Input (µW)	Output (µW)	Input (µW)	Output (µW)	Input (µW)	Output (µW)
Trial #1	0.965	0.875	0.961	0.873	0.960	0.869	0.967	0.889	0.956	0.855
Trial #2	0.961	0.873	0.965	0.877	0.964	0.873	0.964	0.873	0.951	0.851
Trial #3	0.967	0.875	0.967	0.869	0.967	0.875	0.964	0.881	0.960	0.847
Trial #4	0.971	0.872	0.956	0.873	0.956	0.820	0.957	0.877	0.956	0.851
Trial #5	0.965	0.875	0.960	0.871	0.956	0.865	0.961	0.869	0.951	0.855

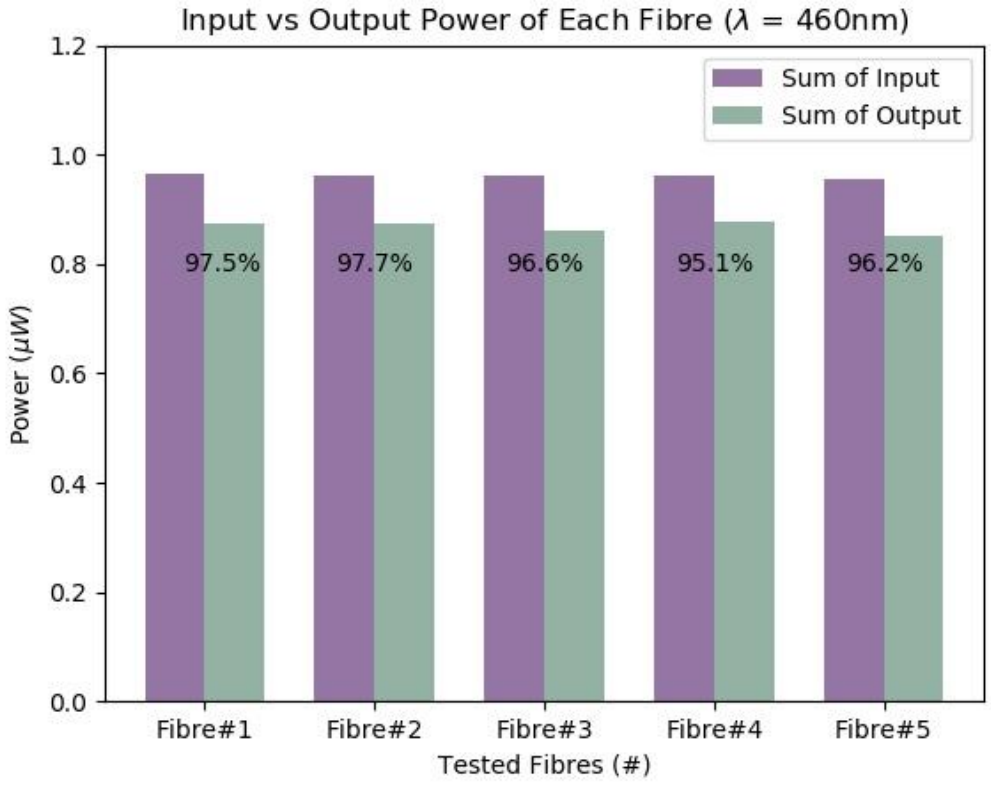

Figure 5.10: Throughput measurement of each fibre using CCD. The text indicates the transmission efficiency of the fibres. (The results exclude the Fresnel reflection loss)

As a result of measuring throughput with a power meter, the transmission efficiency of all five fibres is about 96.6%. In this measurement, Fibre # 2 has the highest transmission efficiency and Fibre # 5 has the lowest transmission efficiency.

5.3.3 Throughput Measurement Comparison with the Power Meter.

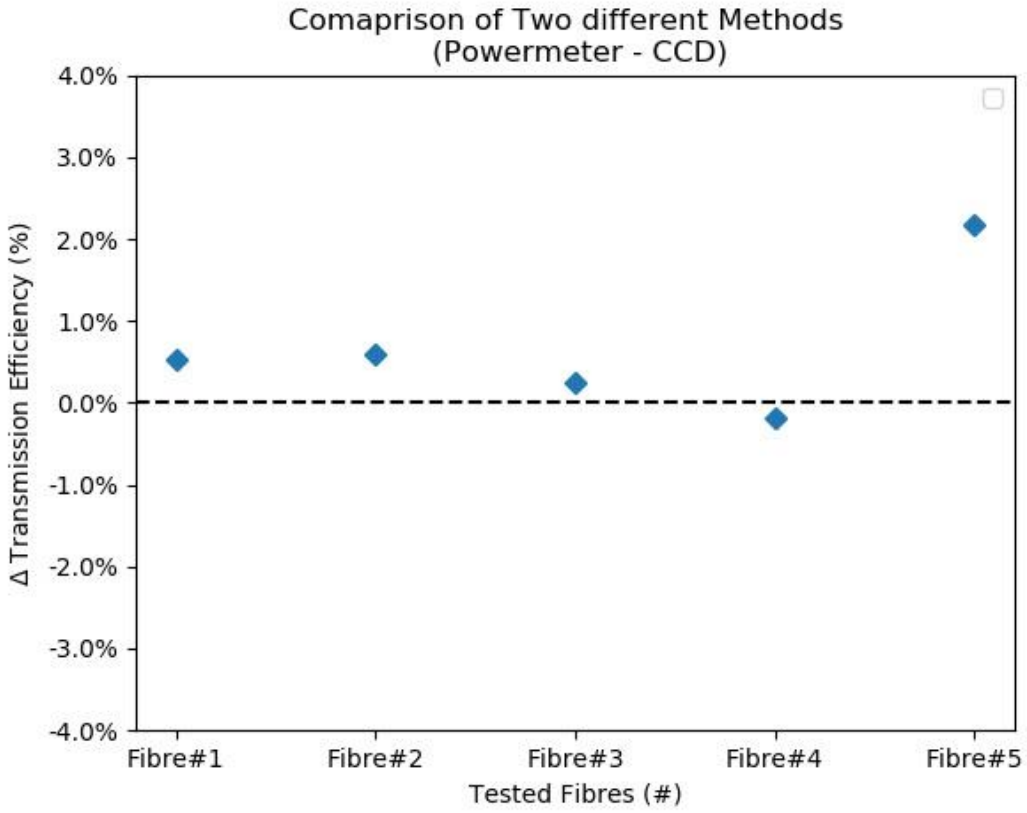

Figure 5.11: Transmission efficiency comparison of two different methods (CCD and power meter)

The two results show that fibres # 1, 2 and 3 have better transmission efficiency than the other two fibres. By comparing the transmission efficiency results of two methods, the maximum difference of fibre # 1, 2, 3 and 4 was less than 0.6%, and the maximum difference of fibres # 5 was more than 2%. Similar results were obtained with throughput measurements from two different methods. As shown in Figure 5.11, results from CCD

camera that compares the input/output far-field image intensity, are highly comparable with results from power meter measurement. However, it has been shown that the method of measuring the transmittance by comparing the intensity of the input image using CCD camera is less efficient than the measurement of the transmission efficiency of the optical fibre through the power meter. This is because the CCD is heavily influenced by the surrounding environment, such as the light coming through windows during the daytime. In addition, the CCD camera requires more correction, such as changes in image processing or camera characteristics (i.e., gain and exposure time). However, similar results were obtained in two different ways, and the difference was not significant, and the difference between the two methods was minimized when experimenting in a completely dark room.

Chapter 6 – Conclusion and Future Work

The Maunakea Spectroscopic Explorer (MSE) design process is well underway and many technology assessment projects are being carried out to examine critical technologies that are deemed high-risk. The MSE Fiber Transmission System (FiTS) consists of 4,332 fibres, grouped into bundles, that require a manufacturing and assembly method that does not degrade the input focal ratio after transmission along the fibre to the output at the spectroscopes. An automated optical test bench was designed, constructed and tested for FRD measurement on typical MSE fibre bundle arrangements. The optical test bench performs the collimated beam, or "ring" test, on MSE candidate fibres to ensure that the science requirement of a FRD of less than 5% is maintained.

The FiTS optical bench system was automated a specially written Python wrapper to control the various bench subsystems. Control of the camera and the rotational stage was performed within the wrapper, the Big FFW, as well as the final post-processing and analysis. The final product is self-contained and compatible with any operating system. The user is only required to enter a range of input light beam injection angles and one camera characteristic (a camera gain) to the Big FFW. In return, the FRD versus incident angle profile is determined for each fibre under test. The Big FFW successfully reduces the time to test individual fibres from hours to minutes. The tests performed using the Big FFW show that the candidate fibres meet the MSE FRD requirements and verified that the Big FFW is a viable alternative to the traditional Ring Test methods.

Two different automated optical test arrangements were designed and implemented for the FRD measurement:

1. Focal ratio degradation measurement of a single fibre

An optical bench system was designed and implemented for measuring the FRD performance of the MSE candidate fibre. For the FRD measurement, new software has been developed that performs the ring test on the candidate fibres with an automated system. The final FRD achieved was 3.7% at f/2 which means that the test system can ensure the MSE science requirements are achieved.

2. Focal ratio degradation measurement of a fibre bundle

A automated optical test bench was designed and implemented for measuring the FRD of the MSE-structure fibre bundle. This fibre bundle consists of five fibres arranged along a small slit similar to the MSE spectroscope input geometry. At the input side, were five individual fibres simulating the input from the MSE Sphinx positioner system. There were linear and angular misalignment issues with the fibre bundle, and so two additional software calibration routines were developed to solve the problem:

- A routine to determine the centre point of any fibre in the bundle. The centre positioning code finds the current position of the light on the CCD screen, and bring the light to the centre of the CCD. It allows illumination of the light to the same area on the CCD screen repeatedly.
- A routine for calibrating the zero position. The zero-calibration code defines the normal incident angle of the fibre. Due to the angular-misalignment, the fibre is slightly tilted, and the normal incident angle of each fibre is different. This code defines the normal incident angle of each fibre and corrects the angle to be 0˚ before starting to perform FRD measurement.
- Fibre bundle case:

1. Blue LED ($\lambda = 460$ nm): The FRD results of all fibres in a bundle fall within the range of 6.5% and 8.5%.
2. Red LED ($\lambda = 625$ nm): The FRD results of the fibres ranged between 7.3% and 9.6%

FRD measurement results for the fibre bundle don't meet the MSE science requirement, however, they are not the exact MSE-candidate fibres. The results do show that FRD can be measured repeatedly and accurately.

- The fully automated system can measure the FRD of one single fibre in less than 2 minutes, including all calibration codes. This fast processing time supports the MSE fibre production schedule (one-cable-per week). The total amount of time for the fibre bundle was measured to be approximately 13minutes. In the MSE project, the cable consists of 76 fibres, so processing time for the cable will be 3hours and 15minutess.

This fully automated optical bench is able to measure the FRD of multiple fibres in a repeatable and accurate manner. This process is critically important for developing the MSE fibre manufacturing and assembly process, where over 4000 fibres must be assembled into discrete bundles. Each fibre in the bundle must be prepared for mating with a discrete Sphinx positioner at the input and, at the output, every fibre in the bundle must be integrated within a slit for light injection into the spectroscope. Any deviation of FRD from the MSE science specification would have disastrous consequences for overall telescope performance. This system will ensure that the manufacture and assembly process maintains the necessary stringent quality control measures.

3. Throughput measurement of high numerical aperture fibre

Another optical bench was designed for measuring the throughput of the MSE candidate fibre and the optical fibre bundle. The throughput of the fibre was measured through two different methods:

1. Using a CCD camera to compare the total amount of intensity of the input and output images.
2. Using the power meter to compare the total power of the input and output beam.

The MSE candidate Fibre case:

- The throughput of the MSE candidate fibre achieved 93% by using CCD.
- The throughput of the MSE candidate fibre through the power meter was 94%.

The fibre bundle case:

- The throughput of the fibre bundle achieved 96% by using CCD.
- The throughput of the fibre bundle through the power meter was 97%.

The throughput results of using CCD camera are in close agreement with the results from the power meter measurement. The maximum difference between CCD and power meter measurements is less than 0.6%

Future Work

The future work should also examine the stability of the FRD measurements for every fibre in a bundle as the bundle is subjected to the types of motions that exactly represent the motions the bundle will experience when installed on the MSE structure. As the telescope moves across the night sky, the azimuth structure could rotate continuously in the range -270° ~ +270°. This motion will subject every fibre in the bundle to a variety of dynamic stresses along the fibre's longitudinal axis (tension) and stresses induced due to a bending radius imposed on the bundle. These dynamic stresses are:

- Twisting of the bundle up to ±180˚.

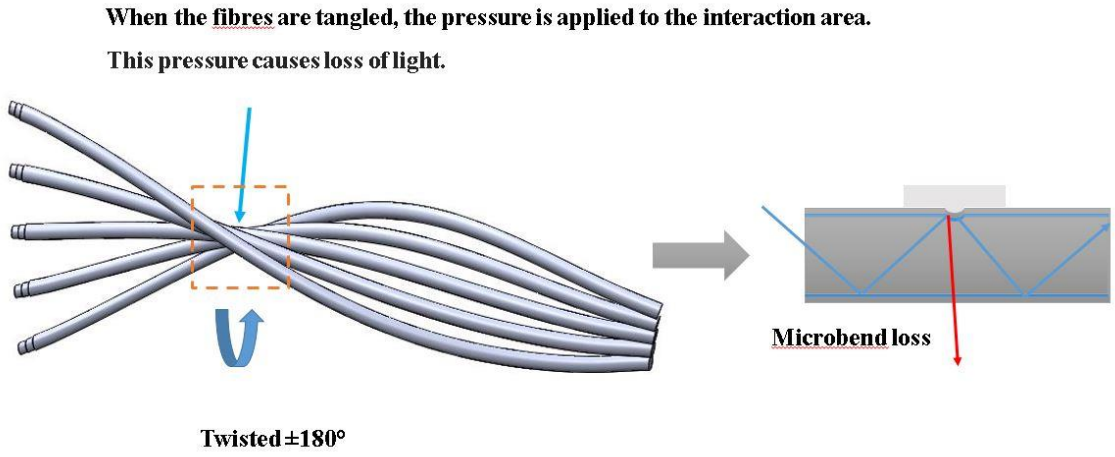

Figure 6.1: An example of stress caused by twisting fibres.

- Rolling up the bundle.

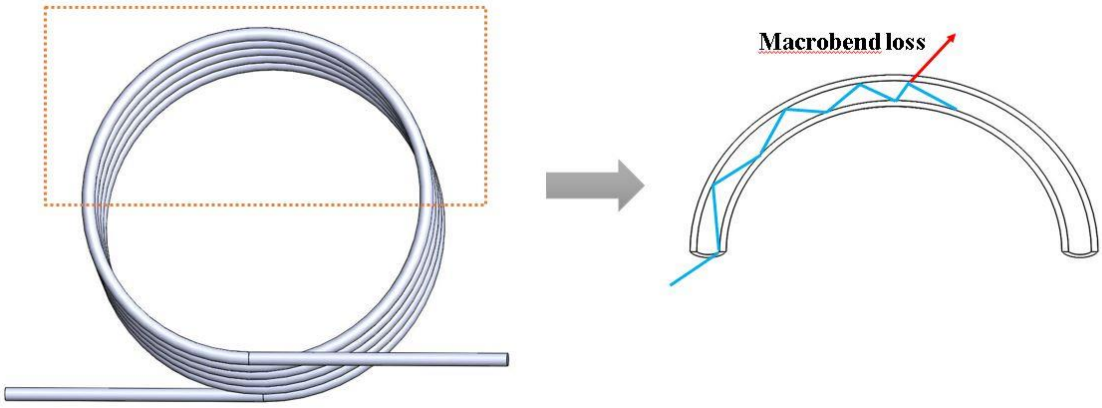

Figure 6.2: An example of stress caused by rolling/bending fibres.

Therefore, a testing mechanism should be developed for assessing the dynamic FRD measurements, on a full-scale fibre bundle prototype. Lastly, the ultimate goal will be to combine the throughput, formed beam and stability tests (with dynamic stresses) into one single automated system for complete and consistent fibre bundle testing.

Bibliography

[1] Venn, Kim, Darren Erickson, David Crampton, Rafal Pawluczyk, Paul Fournier, Patrick Hall, Colin Bradley et al. "MSE FiTS: the ultimate multi-fiber optic transmission system." In *Ground-based and Airborne Instrumentation for Astronomy VII*, vol. 10702, p. 107027S. International Society for Optics and Photonics, 2018.

[2] McConnachie, Alan W., Carine Babusiaux, Michael Balogh, Elisabetta Caffau, Pat Côté, Simon Driver, Aaron Robotham et al. "A concise overview of the Maunakea Spectroscopic Explorer." *arXiv preprint arXiv:1606.00060* (2016).

[3] Saunders, Will, and Peter R. Gillingham. "Optical designs for the Maunakea Spectroscopic Explorer telescope." In *Ground-based and Airborne Telescopes VI*, vol. 9906, p. 990638. International Society for Optics and Photonics, 2016.

[4] Zhang, Kai, Yongtian Zhu, and Zhongwen Hu. "Mauna Kea Spectrographic Explorer (MSE): a conceptual design for multi-object high resolution spectrograph." In *Ground-based and Airborne Instrumentation for Astronomy VI*, vol. 9908, p. 99081P. International Society for Optics and Photonics, 2016.

[5] Pazder, John S., Scott Roberts, Roberto Abraham, Andre Anthony, Murray Fletcher, Tim Hardy, David Loop, and Simon Sun. "WFOS: a wide field optical spectrograph for the Thirty Meter Telescope." In *Ground-based and Airborne Instrumentation for Astronomy*, vol. 6269, p. 62691X. International Society for Optics and Photonics, 2006.

[6] Kelz, Andreas, Francois Hammer, and Pascal Jagourel. "MOSAIC: a Multi-Object Spectrograph for the E-ELT." *arXiv preprint arXiv:1512.00777* (2015).

[7] Goodwin, Michael, Jurek Brzeski, Scott Case, Matthew Colless, Tony Farrell, Luke Gers, James Gilbert et al. "MANIFEST instrument concept and related technologies." In *Ground-based and Airborne Instrumentation for Astronomy IV*, vol. 8446, p. 84467I. International Society for Optics and Photonics, 2012.

[8] Pazder, John, Paul Fournier, Rafal Pawluczyk, and Maaike van Kooten. "The FRD and transmission of the 270-m GRACES optical fiber link and a high numerical aperture fiber for astronomy." In *Advances in Optical and Mechanical Technologies for Telescopes and Instrumentation*, vol. 9151, p. 915124. International Society for Optics and Photonics, 2014.

[9] Carrasco, Esperanza, and Ian R. Parry. "A method for determining the focal ratio degradation of optical fibres for astronomy." *Monthly Notices of the Royal Astronomical Society* 271, no. 1 (1994): 1-12.

[10] Ramsey, Lawrence W. "Focal ratio degradation in optical fibers of astronomical interest." In *Fiber optics in astronomy*, vol. 3, pp. 26-39. 1988.

[11] Bershady, Matthew A., David R. Andersen, Justin Harker, Larry W. Ramsey, and Marc AW Verheijen. "SparsePak: a formatted fiber field unit for the WIYN telescope Bench Spectrograph. I. Design, construction, and calibration." *Publications of the Astronomical Society of the Pacific* 116, no. 820 (2004): 565.

[12] Poppett, C. L., and J. R. Allington-Smith. "The dependence of the properties of optical fibres on length." *Monthly Notices of the Royal Astronomical Society* 404, no. 3 (2010): 1349-1354.

[13] Gloge, D. "Optical power flow in multimode fibers." *Bell System Technical Journal* 51, no. 8 (1972): 1767-1783.

[14] Gambling, W. A., D. N. Payne, and H. Matsumura. "Mode conversion coefficients in optical fibers." *Applied Optics* 14, no. 7 (1975): 1538-1542.

[15] Allington-Smith, Jeremy, Colin Dunlop, Ulrike Lemke, and Graham Murray. "End effects in optical fibres." *Monthly Notices of the Royal Astronomical Society* 436, no. 4 (2013): 3492-3499.

[16] Manset, Nadine, and Jean-Francois Donati. "ESPaDOnS; an Echelle spectropolarimetric device for the observation of stars." In *Polarimetry in Astronomy*, vol. 4843, pp. 425-437. International Society for Optics and Photonics, 2003.

[17] Poppett, C. L., and J. R. Allington-Smith. "Fibre systems for future astronomy: anomalous wavelength–temperature effects." *Monthly Notices of the Royal Astronomical Society* 379, no. 1 (2007): 143-150.

[18] Lee, D., R. Haynes, and D. J. Skeen. "Properties of optical fibres at cryogenic temperatures." *Monthly Notices of the Royal Astronomical Society* 326, no. 2 (2001): 774-780.

Appendix

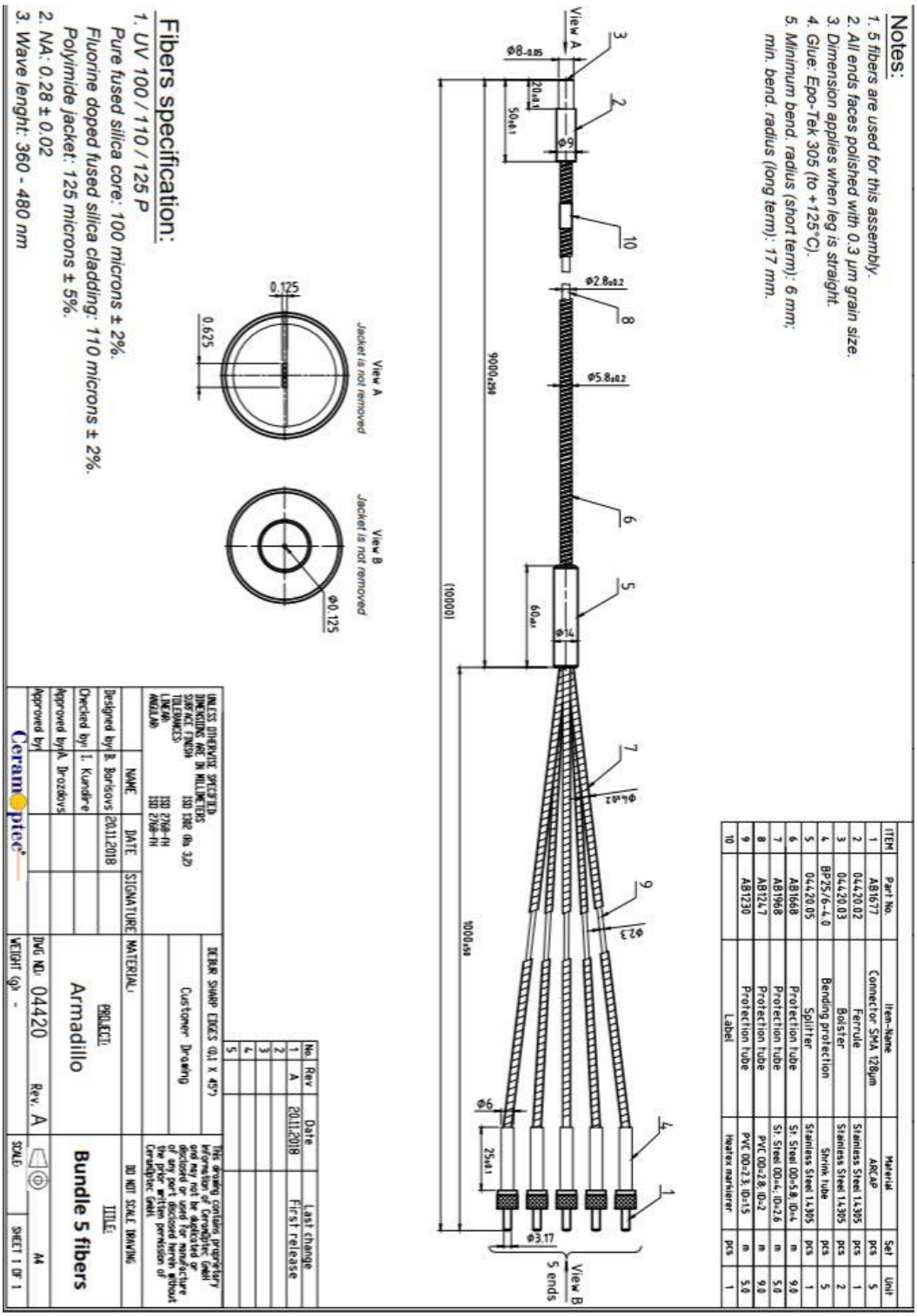
Notes:
1. 5 fibers are used for this assembly.
2. All ends faces polished with 0.3 µm grain size.
3. Dimension applies when leg is straight.
4. Glue: Epo-Tek 305 (to +125°C).
5. Minimum bend. radius (short term): 6 mm;
min. bend. radius (long term): 17 mm.
Fibers specification:
1. UV 100 / 110 / 125 P
Pure fused silica core: 100 microns ± 2%.
Fluorine doped fused silica cladding: 110 microns ± 2%.
Polyimide jacket: 125 microns ± 5%.
2. NA: 0.28 ± 0.02
3. Wave lenght: 360 - 480 nm
View A
Jacket is not removed
View B
Jacket is not removed
5 ends
Armadillo
Bundle 5 fibers
04420
Rev. A
A4
SHEET 1 OF 1